Available online at www.sciencedirect.com
SCIENCE DIRECT®
International Journal of Heat and Mass Transfer 49 (2006) 2684–2702
International Journal of HEAT and MASS TRANSFER
www.elsevier.com/locate/ijhmt

Numerical simulation of natural convection in a horizontal enclosure with a heat-generating conducting body

Jae Ryong Lee, Man Yeong Ha *

School of Mechanical Engineering, Pusan National University, San 30, Chang Jeon Dong, Kum Jeong Gu, Pusan 609-735, Republic of Korea

Received 17 July 2005; received in revised form 9 January 2006
Available online 22 March 2006

Abstract

The physical model considered here is a horizontal layer of fluid heated below and cold above with heat-generating conducting body placed at the center of the layer. The dimensionless thermal conductivities of body considered in the present study are 0.1, 1 and 50. The dimensionless temperature difference ratios considered are 0.0, 0.25, 2.5 and 25. Two-dimensional solution for unsteady natural convection is obtained using an accurate and efficient Chebyshev spectral methodology for variety of Rayleigh number from 10^3 to 10^6. Multi-domain technique is used to handle square-shaped heat-generating conducting body. The fluid flow, heat transfer and time- and surface-averaged Nusselt number are investigated for various ranges of Rayleigh number, thermal conductivity ratio and dimensionless temperature difference ratio. The results for the case of conducting body with heat generation are also compared to those without heat generation to see the effects of heat generation from the conducting body on the fluid flow and heat transfer in the enclosure.

1. Introduction

Rayleigh–Bénard convection in a horizontal layer of fluid confined between two parallel plates, with the bottom plate heated and the top one cooled, has been well studied for over a century. It has been well established that for the isothermal boundary condition the horizontal layer of fluid becomes unstable above a Rayleigh number of 1708 and convective motion sets in the form of steady convective rolls of aspect ratio (width to height) of about 2 [1]. With increasing Rayleigh number the flow undergoes a sequence of instabilities and eventually transitions to a turbulent state above a Rayleigh number of about 10^7 [2,3].

The geometries that arise in engineering applications, however, are more complicate than a simple horizontal layer of convecting fluid. Ha et al. [4]. considered the problem of natural convection in a square enclosure with isothermal top and bottom boundaries and various conditions of thermal boundary of interior body, and also, an aspect ratio effect of given enclosure with equi-spaced array of bodies was investigated by Lee et al. [5], in which they concluded that the transition of flow from quasi-steady up to unsteady convection depends on the presence of bodies and aspect ratio effect of the cell.

However, a body considered was not calculated but treated a rigid wall. In order to consider interior body, many numerical studies have conducted for couples of decades. One of the earliest systematic numerical investigations of this problem was by House et al. [6] who considered the influence of a centered conducting body on natural convection within an enclosure. For given Ra and Pr, an existence of conducting body with thermal conductivity ratio less than unity makes heat transfer enhanced. Deng and Tang [7] defined a heat function to visualize the heat and fluid flow in an air filled square cavity over a wide range of $Ra = 10^3$–10^6, and those for conjugate natural convection/heat conduction where the conduction effect of solid body on heat transfer is studied. Moreover, a phenomenon of free convection with another heat source is quite interesting and has been studied vigorously. Oh et al. [8] investigated the steady natural convection processes when a

* Corresponding author. Tel.: +82 51 510 2440; fax: +82 51 512 9835.
E-mail address: myha@pusan.ac.kr (M.Y. Ha).

0017-9310/$ - see front matter © 2006 Elsevier Ltd. All rights reserved.
doi:10.1016/j.ijheatmasstransfer.2006.01.010

Nomenclature

A^*	area ratio ($= W^2/L^2$)
C_p	constant pressure specific heat
g	gravity
k	dimensionless thermal conductivity ($= k_s/k_f$)
L	length of the enclosure
$\mathbf{n}$	vector normal to surface
Nu	local Nusselt number
$\overline{Nu}$	surface-averaged Nusselt number
$\langle\overline{Nu}\rangle$	time- and surface-averaged Nusselt number
p	dimensionless pressure
Pr	Prandtl number
$\dot{q}$	heat generation per unit surface
Ra	Rayleigh number
t	dimensionless time
t^*	dimensional time
t_p	period of time integration
$\mathbf{u}$	dimensionless velocity
$\mathbf{u}^*$	dimensional velocity
$\mathbf{x}$	dimensionless coordinate vector
$\mathbf{x}^*$	dimensional i-directional coordinate
α	dimensionless thermal diffusivity ($= \alpha_s/\alpha_f$)
β	thermal expansion coefficient
ρ	dimensionless density
C_p	dimensionless specific heat
ΔT^*	temperature-difference ratio ($= (\dot{q}W^2/k_f)/(T_h - T_c)$)
v_f	kinematic viscosity of fluid
θ	dimensionless temperature

Subscripts/superscripts

body	body
c	cold
f	fluid
h	hot
p	period
s	solid

temperature difference exists across the enclosure and, at the same time, a conducting body generates heat within the enclosure. Under this situation, the flow inside the enclosure is driven by two temperature differences: a temperature difference across the enclosure and a temperature difference caused by heat source. A ratio of these two temperature differences is a very important factor to decide the heat transfer and flow characteristics of the enclosure. They investigated the effects of Rayleigh numbers and temperature difference ratio on variations of streamlines, isotherms, heat lines and the averaged Nusselt numbers on the hot and cold walls. Ha and Jung [9] conducted a comprehensive numerical study to investigate three-dimensional steady, conjugate heat transfer of natural convection and conduction in a vertical cubic enclosure within which a centered, cubic, heat-conducting body generates heat. The presence of a cubic conducting body in a cubic enclosure results in a larger variation of the local Nusselt number at the hot and cold walls in the z-direction.

However, there is little information about natural convection processes when a heat-conducting body exists within a horizontal layer of fluid confined between the hot bottom and cold top walls. The horizontal enclosure with heat-generating body can be applied in many engineering/scientific fields such as solar energy collection system, cooling of nuclear power system, cooling of heat-generating components in the electrical industry and the flows in rooms due to thermal energy sources. We consider a horizontal layer of fluid, heated from below and cooled from above, with a heat-generating conducting square body at the center of the layer. Rayleigh number varies from 10^3 up to 10^6. In order to consider the effect of thermal conductivity ratio between solid body and fluid layer, we have chosen the value to be 0.1, 1 and 50. The fluid flow, heat transfer and time- and surface-averaged Nusselt number are investigated for various ranges of Rayleigh number and thermal conductivity ratio. We considered four different levels of heat generation of interior body: 0.0 (no heat generation), 0.25, 2.5 and 25. The results with heat generation are compared to those without heat generation to see the effects of heat generation on the fluid flow and heat transfer in the enclosure.

2. Numerical methodology

A schematics of the system considered in present paper is shown in Fig. 1. The system consists of a square enclosure with sides of length L, within which another square body

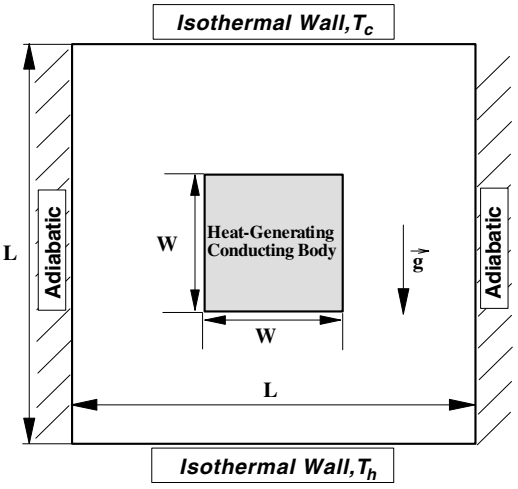

Fig. 1. Schematics of the system.

with sides of length W, is centered and has a thermal conductivity of k_s and a heat generation per unit volume of $\dot{q}$. The bottom wall is kept at a constant high temperature of T_h, whereas the top wall is kept at a constant low temperature of T_c. The left and right side walls are assumed to be insulated. In this study, we assume that the radiation effects can be taken to be negligible. The fluid properties are also assumed to be constant, except for the density in the buoyancy term, which follows the Boussinesq approximation. The gravitational acceleration acts in the negative y-direction. Thus, in the present study, we observe the fluid flow and thermal fields for the natural convection in an enclosure with heat-generating conducting body at the center.

We solve the continuity, Navier–Stokes and energy equations in their non-dimensional forms defined as

$$\nabla \cdot \mathbf{u} = 0 \tag{1a}$$

$$\frac{\partial \mathbf{u}}{\partial t} + \mathbf{u} \cdot \nabla \mathbf{u} = -\nabla p + Pr \nabla^2 \mathbf{u} + Ra\, Pr \theta_f \mathbf{k}_2 \tag{1b}$$

$$\frac{\partial \theta_f}{\partial t} + \mathbf{u} \cdot \nabla \theta_f = \nabla^2 \theta_f \tag{1c}$$

$$\frac{\partial \theta_s}{\partial t} = \alpha \nabla^2 \theta_s + \frac{\Delta T}{(\rho C_p) A} \tag{1d}$$

The dimensionless variables in the above equations are defined as

$$t = \frac{t^* \alpha_f}{L^2}, \quad \mathbf{x} = \frac{\mathbf{x}^*}{L}, \quad \mathbf{u} = \frac{\mathbf{u}^* L}{\alpha_f}, \quad P = \frac{P^* L^2}{\rho_f \alpha_f^2}, \quad \theta = \frac{T - T_c}{T_h - T_c} \tag{2}$$

In the above equations, the superscript $*$ represents the dimensional variables, and dimensionless parameters are defined as

$$Pr = \frac{\nu}{\alpha_f}, \quad Ra = \frac{g\beta L^3 (T_h - T_c)}{\nu \alpha_f}, \quad \Delta T = \frac{\dot{q} W^2 / k_f}{T_H - T_C},$$
$$\alpha = \frac{\alpha_s}{\alpha_f}, \quad \rho C_p = \frac{(\rho C_p)_s}{(\rho C_p)_f}, \quad A = \frac{W^2}{L^2} \tag{3}$$

In the simulations to be reported here the area ratio, A is 1/9 and the Prandtl number, Pr is taken to be 0.7 corresponding to air. The Rayleigh number, Ra, and the temperature difference ratio, ΔT, are varied over the range of 10^3–10^6 and 0–25, respectively. The values of dimensionless thermal diffusivity, α, for different values of k are 0.001 for $k = 0.1$, 1 for $k = 1$ and 0.05 for $k = 50$, respectively.

For the boundary conditions, the velocities are set to zero for all solid walls. The temperature boundary conditions and the conditions at the fluid/body interfaces are as follows;

$$\text{At } x = 0 \text{ and } 1; \quad \frac{\partial \theta}{\partial x} = 0 \tag{4a}$$

$$\text{At } y = 0; \quad \theta = 1 \tag{4b}$$

$$\text{At } y = 0; \quad \theta = 0 \tag{4c}$$

$$\text{At fluid/body interface;} \quad \theta_s = \theta \text{ and } \frac{\partial \theta}{\partial n} = k \frac{\partial \theta_s}{\partial n} \tag{4d}$$

where $k(= k_s/k_f)$ is thermal conductivity ratio between solid body and fluid and $\mathbf{n}$ is a vector normal to solid surface. We considered different k values of 0, 0.1, 1 and 50 in the present calculation.

A spectral multi-domain methodology is used for the spatial discretization along the x- and y-directions [10]. In this technique the overall computational domain is subdivided into a number of smaller rectangular subdomains. Within each subdomain a local spectral Chebyshev discretization is defined [11]. Fig. 1 shows the computational geometry involving 9 subdomains in the x–y plane, with each subdomain resolved by 31×31 points. The grid points are the Gauss–Lobatto points corresponding to Chebyshev expansion within each subdomain and are therefore non-uniformly distributed. Grid independence of the solution has been confirmed with additional simulations on much finer grids up to 51×51 points [5], and also, we have conducted grid resolution test between coarse and fine grid distribution for similar geometry [12] and obtained grid independency for this study.

A two-step time-split scheme is used to advance the flow field. First, the velocity is advanced from time level 'n' to an intermediate level by solving the advection–diffusion equation

$$\frac{\mathbf{u}_* - \mathbf{u}_n}{\Delta t} = \frac{Pr}{2}\left[\nabla^2 \mathbf{u}_* + \nabla^2 \mathbf{u}_n\right] + \left[\frac{23}{12}\mathbf{NL}_n - \frac{16}{12}\mathbf{NL}_{n-1} + \frac{5}{12}\mathbf{NL}_{n-2}\right] \tag{5a}$$

where $\mathbf{u}_*$ is the intermediate level velocity and $\mathbf{NL}$ represents the non-linear and buoyancy terms defined as

$$\mathbf{NL} = \mathbf{u} \cdot \nabla \mathbf{u} - Ra\, Pr\, \theta_f \mathbf{k}_2 \tag{5b}$$

In the advection–diffusion step, the non-linear and buoyancy terms are treated explicitly using the third-order Adams–Bashforth scheme. The diffusion terms are treated implicitly using the Crank–Nicholson scheme as given below:

$$\left|\nabla^2 \mathbf{u} - \frac{\mathbf{u}}{\Delta t} \times \frac{2}{Pr}\right|_* = \left|\frac{2}{Pr}\left[\frac{23}{12}\mathbf{NL}_n - \frac{16}{12}\mathbf{NL}_{n-1} + \frac{5}{12}\mathbf{NL}_{n-2}\right] - \frac{\mathbf{u}}{\Delta t} \times \frac{2}{Pr} - \nabla^2 \mathbf{u}\right|_n \tag{5c}$$

The solution of Eq. (5c) determines the velocity $\mathbf{u}_*$ at the intermediate time step. Then a Poisson equation for pressure is solved fully implicitly as given below:

$$\nabla^2 p_{n+1} = \frac{1}{\Delta t} \nabla \cdot \mathbf{u}_* \tag{5d}$$

The final divergence-free velocity field at '$n+1$' is obtained with the following pressure-correction step

$$\mathbf{u}_{n+1} = \mathbf{u}_* - \Delta t\ \nabla p_{n+1} \tag{5e}$$

The above correction guarantees zero divergence at all the points where the pressure Poisson equation (5d) is satisfied. After obtaining the velocity field, the temperature field is

advanced in a similar manner with the third-order Adams–Bashforth scheme for the advection term (denoted below as AD) and the Crank–Nicholson scheme for the diffusion term

$$\frac{\theta_{n+1}-\theta_n}{\Delta t}=\frac{1}{2}\left[\nabla^2\theta_{n+1}+\nabla^2\theta_n\right]+\left[\frac{23}{12}\mathrm{AD}_n-\frac{16}{12}\mathrm{AD}_{n-1}+\frac{5}{12}\mathrm{AD}_{n-2}\right] \tag{5f}$$

where **AL** represents the non-linear terms defined as

$$\mathbf{AL}=\mathbf{u}\cdot\nabla\theta \tag{5g}$$

The above numerical scheme thus requires the solution of a Helmholtz equation for each component of the intermediate velocity (5a), a Poisson equation for pressure (5d) and a Helmholtz equation for the temperature field (5f). In the context of the present spectral multi-domain technique these elliptic equations are solved using a patching technique [11]. The discretized version of the elliptic equations is solved at the interior grid points and at the boundary points appropriate boundary conditions are enforced. At the interface grid points along the interior interface of the subdomains the strong form of the patching condition that requires C1 continuity (continuity of the function as well of the normal derivative) is enforced. The resulting discretized linear system lends itself to solution through influence matrix technique.

The influence matrix technique can be briefly explained as follows [13]. First, as a preprocessing step an influence matrix is computed, inverted and stored for repeated use each time step. Each column of the influence matrix is formed by the gradient mismatch at all the interface points resulting from a unit Dirichlet condition placed at one of the interface points. The entire influence matrix is assembled by unit forcing placed at each of the interface points, one at a time. At each time step, as the first pass the elliptic (Helmholtz or Poisson) equations are solved independently within each subdomain with zero Dirichlet boundary condition at the interface points. The resulting gradient mismatch in conjunction with the inverse of the influence matrix is used to obtain the correct interface value that will result in C1 continuity. The elliptic equation is solved once again with the appropriate interface value to get the final solution. We use singular value decomposition in solving the influence matrix during the pressure Poisson equation. In this technique the mean pressure (averaged over the volume) is set to zero at each time and any other spurious pressure modes, which might arise from the space of polynomials used for pressure representation, are nullified as well.

At the solid boundaries the following boundary conditions are applied for the intermediate velocity

$$\mathbf{u}_*|_{\mathrm{wall}}\cdot\mathbf{n}=0 \quad \text{and} \quad \mathbf{u}_*|_{\mathrm{wall}}\cdot\mathbf{t}=\left(\frac{3}{2}\nabla p_n-\frac{1}{2}\nabla p_{n-1}\right)_{\mathrm{wall}}\cdot\mathbf{t} \tag{6}$$

where **n** is the unit vector normal to the wall and **t** represents the two orthogonal unit vectors tangential to the wall. In the context of the time-split scheme, the appropriate pressure boundary condition to be applied at the solid boundaries is the homogeneous Neumann condition ($\nabla p\cdot\mathbf{n}=0$). The above boundary conditions along with (5e) exactly satisfy the no-penetration condition at the solid walls and maintain the tangential slip velocity to be nearly zero at $O(\Delta t^3)$.

Owing to viscous scaling the flow velocity is a strong function of Rayleigh number. Correspondingly the time step employed in the simulations are very small and dependent on the Rayleigh number, with Δt ranging from 10^{-3} to 10^{-6} as Ra increases from 10^3 to 10^6. The simulations are typically run on a PC cluster and each high Rayleigh number simulation at $Ra=10^6$ takes about 4 h of CPU time for the unit cell.

Once the velocity and temperature fields are obtained, the local, surface-averaged, time-averaged, and time-and-surface-averaged Nusselt number are defined as

$$Nu=\left.\frac{\partial\theta}{\partial n}\right|_{\mathrm{wall}},\quad \overline{Nu}=\frac{1}{W}\int_0^W Nu\,\mathrm{d}S,\quad \langle Nu\rangle=\frac{1}{t_\mathrm{p}}\int_0^{t_\mathrm{p}} Nu\,\mathrm{d}t,$$
$$\langle\overline{Nu}\rangle=\frac{1}{t_\mathrm{p}}\int_0^{t_\mathrm{p}}\overline{Nu}\,\mathrm{d}t \tag{7}$$

where n is the normal direction to the walls, W is the horizontal extent of the computational domain and t_p is the period of time integration. The above quantities are separately computed for the cold top and the hot bottom walls. The present multi-domain spectral methodology and the computer code used here have been thoroughly validated by comparing results with those of de Vahl Davis [14] and House et al. [6] for the case of a vertical enclosure and with those of Lipps [2] for the case of a horizontal enclosure. For Rayleigh numbers of 10^3, 10^4, 10^5 and 10^6 the benchmark results on surface-averaged Nusselt number obtained by de Vahl Davis [14] are 1.118, 2.243, 4.519 and 8.800. The corresponding results obtained with the present code using 9 subdomains with 31×31 grid points resolving each subdomain are, respectively, 1.118, 2.246, 4.525 and 8.821, yielding less than 0.25% difference, even at the highest Rayleigh number considered. The problem of natural convection in a vertical enclosure with an interior conducting body studied by House et al. [6] was also considered with the present code. The Nusselt number at the hot wall obtained by House et al. [6] for $Ra=10^5$with two different body-to-fluid thermal conductivity ratios of 0.2 and 5.0 are, respectively, 4.324 and 4.624, for a dimensionless body size of 1/2. The corresponding results obtained with the present code using 9 subdomains with 31x31 grid points resolving each subdomains are 4.324 and 4.631. Again the errors are less than 0.15%.

3. Results and discussion

3.1. $k = 0.1$

Fig. 2 shows time-averaged isotherms and streamlines for different values of ΔT and Rayleigh numbers when

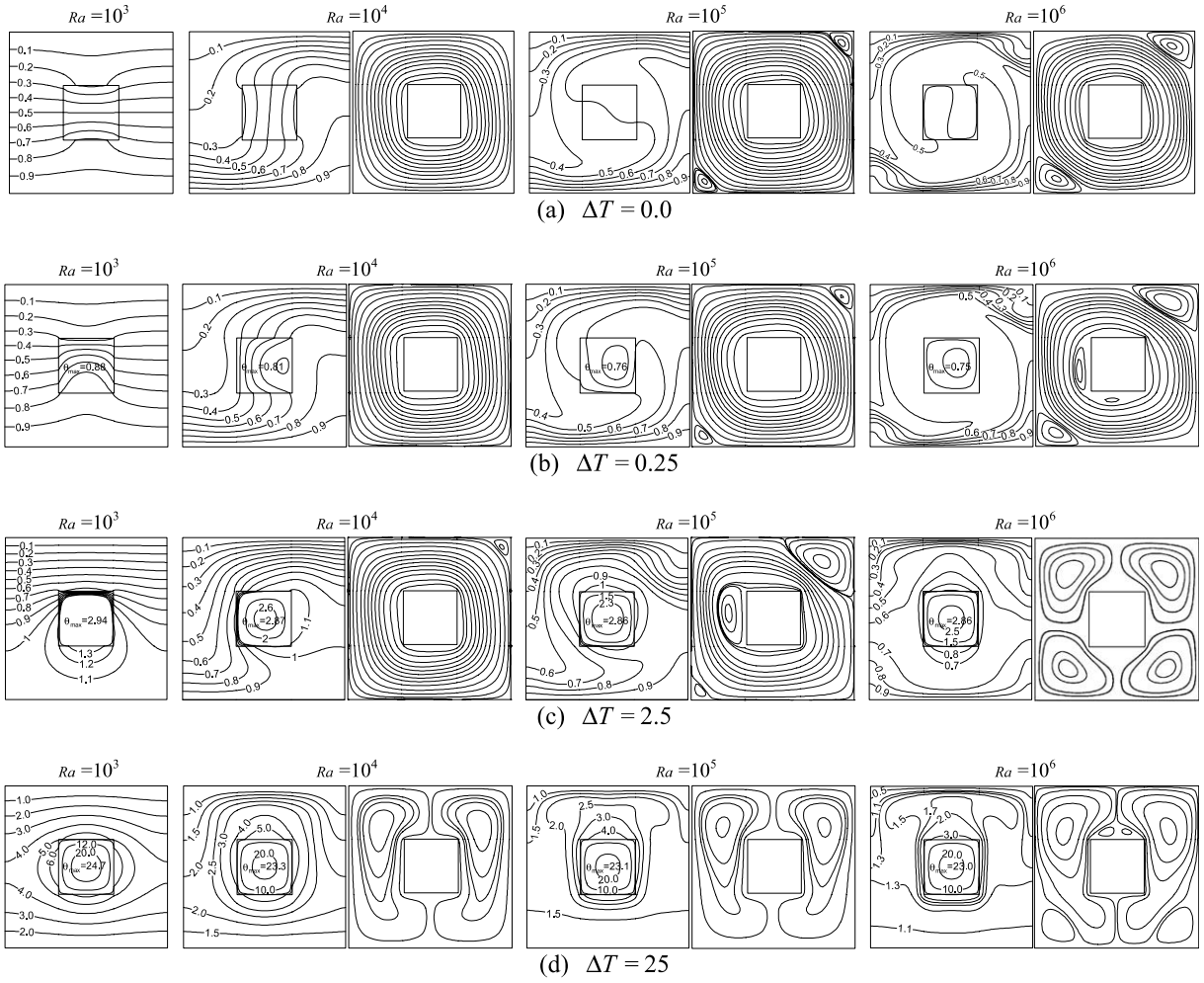

Fig. 2. Time-averaged isotherms and streamlines for different values of ΔT and Rayleigh number when $k = 0.1$.

$k = 0.1$. Fig. 3 shows the corresponding surface-averaged Nusselt numbers at hot bottom and cold top walls as a function of time. When $k = 0.1$, the thermal conductivity of fluid is ten times larger than that of heat generating conducting body. The value of maximum temperature, $\theta_{\max}$, in the enclosure increases with increasing ΔT and decreases slightly with increasing Rayleigh number.

3.1.1. $Ra = 10^3$

When $Ra = 10^3$, heat transfer in the enclosure is mainly governed by the conduction mode. When $\Delta T = 0$ corresponding to the case with no heat generation in the conducting body, the thermal gradient around the top wall is the same as that around the bottom wall and as a result the heat transfer rate from the hot bottom wall to the fluid is also the same as that from the fluid to the cold top wall. When $\Delta T \neq 0$, the temperature in the conducting body increases and heat is transferred from the conducting body to the fluid, due to heat generation from the conducting body.

When $\Delta T = 0.25$, isotherms move upwards due to heat transfer from the body, the thermal gradient at the top wall becomes larger than that at the bottom wall and as a result the amount of heat transferred from the fluid to the top cold wall is larger than that from the bottom hot wall to the fluid, compared to almost same thermal gradients and heat transfer rates at the top and bottom walls when $\Delta T = 0$. The maximum temperature at $\Delta T = 0.25$ is about $\theta_{\max} \approx 0.88$, which is less than the bottom hot wall temperature of $\theta = 1$.

When ΔT is increased to 2.5, the temperature in the conducting body becomes larger than the hot wall temperature with $\theta_{\max} \approx 2.94$ and the temperature of fluid around the bottom hot wall is close to the hot wall temperature. Thus the thermal gradient at the top wall and heat transfer rates from the fluid to the top wall increase more with increasing ΔT from 0.25 to 2.5. However, the thermal gradient around the bottom wall becomes very small and heat transfer rate approaches to the value of zero.

When ΔT is increased further to 25, the temperature in the conducting body keeps increasing with $\theta_{\max} \approx 24.7$ and the temperature of fluid is larger than the bottom hot wall temperature ($\theta = 1$). As a result heat at the bottom wall for $\Delta T = 25$ is transferred from the fluid to the hot wall, which is the opposite direction compared to the cases of $\Delta T = 0$, 0.25 and 2.5. This result shows that heat transfer

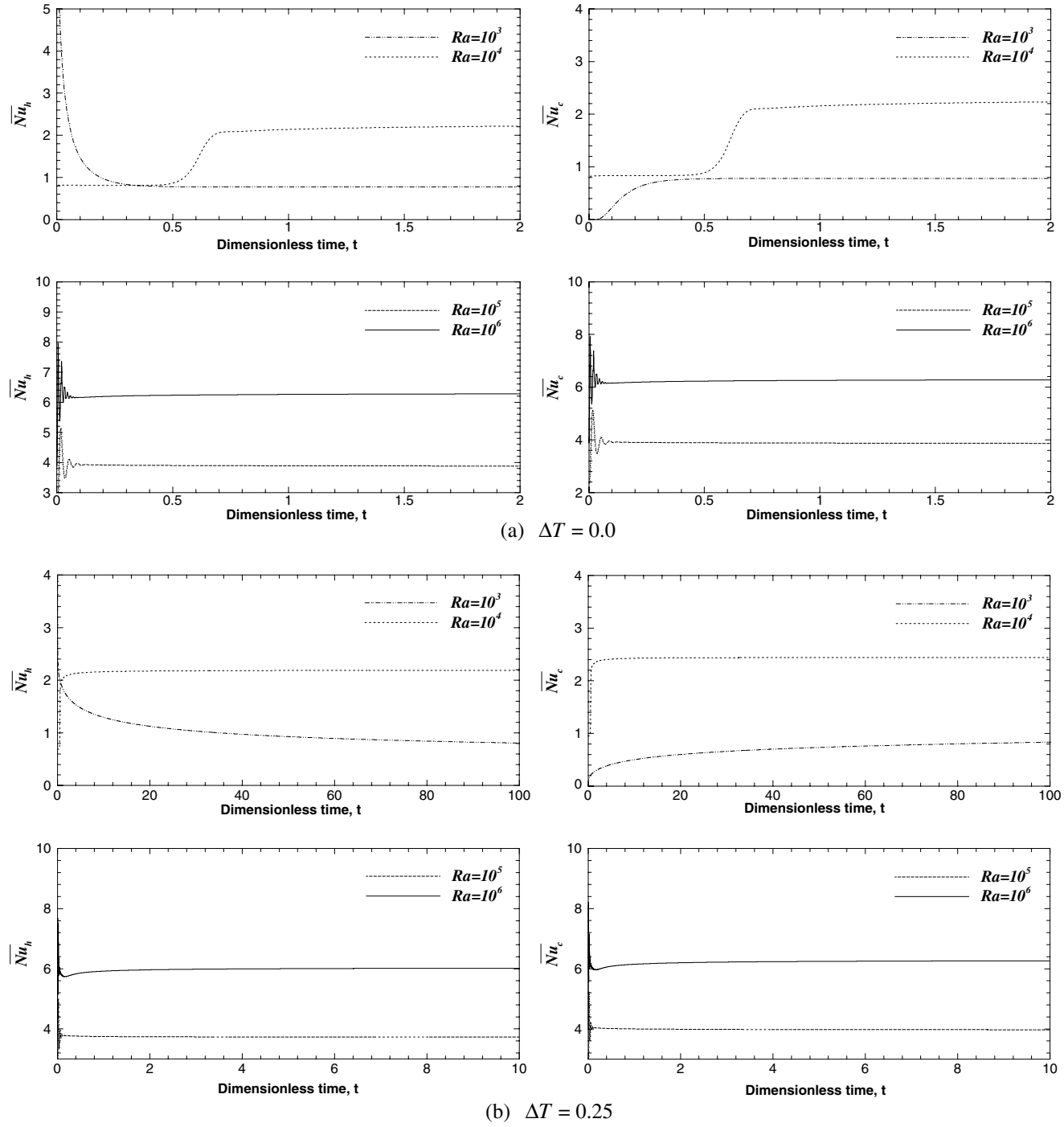

Fig. 3. Surface-averaged Nusselt number at the bottom hot and top cold walls as a function of time for different values of ΔT and Rayleigh number when $k = 0.1$.

for $\Delta T = 0$ is governed by the temperature difference between the hot and cold wall temperatures, whereas that for $\Delta T = 25$ is governed by heat generation from the conducting body.

3.1.2. $Ra = 10^4$

When $Ra = 10^4$, we can observe streamlines and isotherms circulating around the body due to the effect of convection, compared to the pure conduction mode when $Ra = 10^3$. When $\Delta T = 0$ and 0.25, streamlines and their corresponding isotherms circulate around the conducting body in the counterclockwise direction, because the convective heat transfer is governed by the temperature difference between the hot bottom and cold top walls. Because the amount of heat generation from the body is not large when $\Delta T = 0.25$, the distribution of isotherms for $\Delta T = 0.25$ is generally similar to that for $\Delta T = 0$, except the small difference around the conducting body.

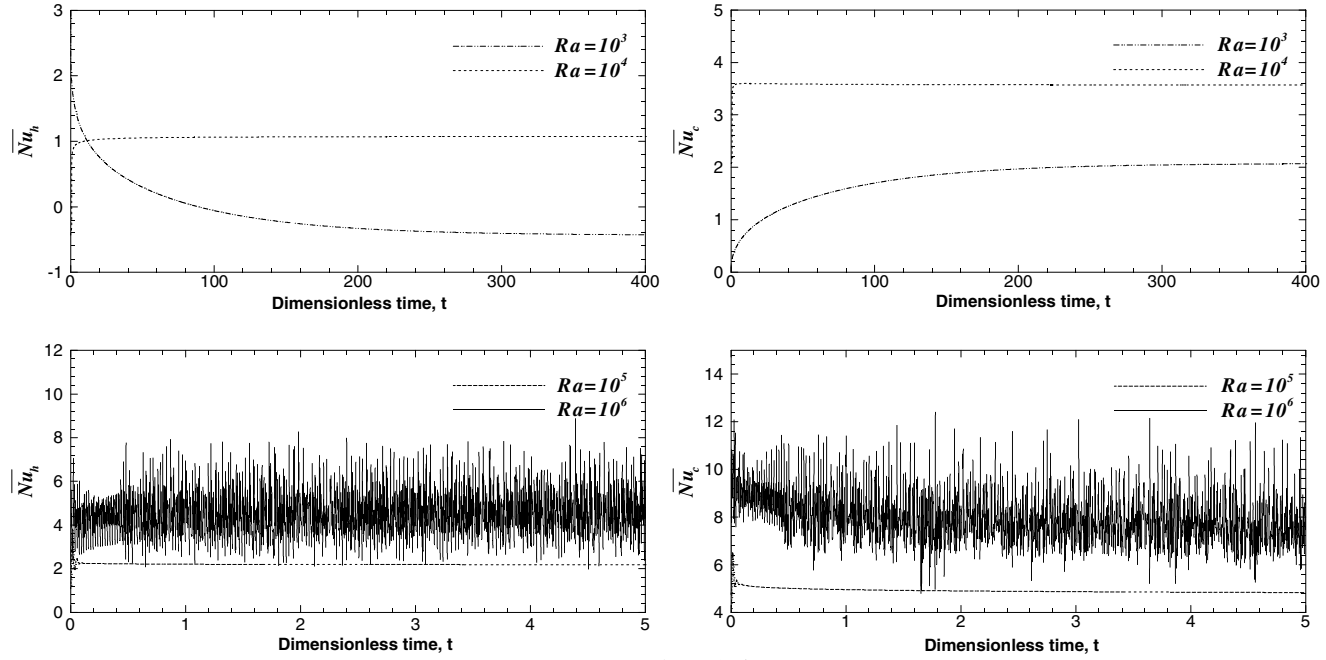

(c) $\Delta T = 2.5$

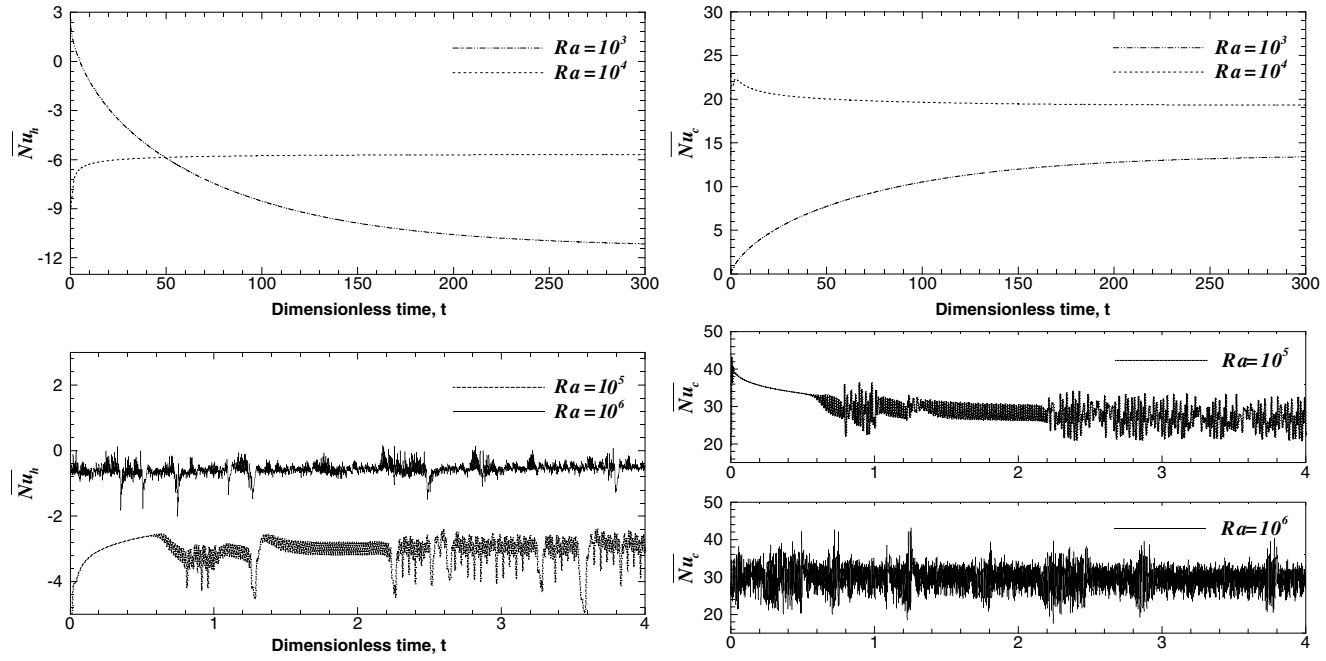

(d) $\Delta T = 25$

Fig. 3 (*continued*)

If ΔT increases to 2.5, the effect of heat generation from the conducting body starts to work. The upwelling flow caused by heat generation and the counter-clockwisely circulating flow caused by the temperature difference between the top and bottom walls have the subtracted effect in the right channel and added effect in the left channel. As a result, when $\Delta T = 2.5$, isotherms in the left channel circulate further in the counter-clockwise direction whereas the circulation of isotherms in the right channel to the counter-clockwise direction is hindered, resulting in the denser thermal gradient around the top wall and smaller one around the bottom wall, compared to the distribution of isotherms and their gradient when $\Delta T = 0$ and 0.25.

When ΔT increases further to 25, the convective heat transfer in the enclosure is governed by heat generation from the conducting body and the temperature of fluid around the center is higher than that around the adiabatic side walls at the same elevation due to the strong effect of

heat generation. As a result we can observe the upwelling flow in the core region and the downwelling flow in the outer vertical adiabatic walls, resulting in the formation of a pair of vortices in the enclosure at $\Delta T = 25$, compared to the formation of a single cell of vortices when $\Delta T = 0$, 0.25 and 2.5. Because the temperature of fluid in the enclosure is higher than the bottom hot wall temperature at $\Delta T = 25$, heat is transferred from the fluid to the bottom wall, whose direction is opposite to the direction of heat transfer for the cases of $\Delta T = 0$, 0.25 and 2.5.

3.1.3. $Ra = 10^5$

When $Ra = 10^5$, because the velocity magnitude caused by the temperature difference between the bottom hot and top cold walls becomes larger than that when $Ra = 10^4$, the thickness of the thermal boundary layer around walls becomes thinner and thermal gradient becomes larger generally than those when $Ra = 10^4$, for all different values of ΔT considered.

When $\Delta T = 0$ and 0.25 for $Ra = 10^5$, the fluid flow and heat transfer are mainly governed by the temperature difference between the bottom hot and top cold walls, similar to those for $Ra = 10^4$. Thus, when $\Delta T = 0$ and 0.25 for $Ra = 10^5$, the main flow circulates in the counter-clockwise direction around the conducting body with small secondary vortices formed on the right top and left bottom corners and the corresponding isotherms also circulate to the same direction by following the flow field, which is similar to the case of $Ra = 10^4$ for the same ΔT. When $Ra = 10^5$, isotherms for $\Delta T = 0.25$ have similar shapes to those for $\Delta T = 0$ and the small difference is observed around the conducting body.

When $\Delta T = 2.5$, the effects of both upwelling flow caused by heat generation and counter-clockwisely circulating flow caused by the temperature difference between the top and bottom walls on the distribution of isotherms and streamlines work together in the enclosure for both cases of $Ra = 10^4$ and 10^5. However, because the effect of counter-clockwisely circulating flow caused by the bottom and top wall temperature difference at $Ra = 10^5$ is larger than that at $Ra = 10^4$ for the same value of $\Delta T = 2.5$, the isotherms for $Ra = 10^5$ rotate more in the counter-clockwise direction than those for $Ra = 10^4$. The size of secondary vortices at the right top corner for $\Delta T = 2.5$ becomes much bigger than that for $\Delta T = 0$ and 0.25. The size of secondary vortices at the left bottom corner for $\Delta T = 2.5$ becomes slightly smaller compared to that for $\Delta T = 0$ and 0.25. We can also observe the tertiary vortices which are circulating in the clockwise direction and formed at the left side of conducting body.

When ΔT increases further to 25 at $Ra = 10^5$, the thermal fields do not show final steady state but unsteady fashion as shown in Fig. 3(d). Thus isotherms and streamlines shown in Fig. 2(d) for $Ra = 10^5$ at $\Delta T = 25$ are time-averaged temperature and velocity fields. When $\Delta T = 25$, because of much stronger effect of heat generation from the conducting body at $Ra = 10^5$, we can observe a pair of vortices formed in the enclosure, similar to the case of $Ra = 10^4$.

3.1.4. $Ra = 10^6$

When $Ra = 10^6$, the velocity magnitude caused by the temperature difference between the bottom hot and top cold walls increases more than that when $Ra = 10^5$. Thus, when $\Delta T = 0$ and 0.25 for $Ra = 10^6$, isotherms rotate more to the counter-clockwise direction, the thickness of thermal boundary layer on the walls becomes much thinner, and the size of secondary vortices formed on the right top and left bottom corners becomes larger, compared to those when $Ra = 10^5$ for the same values of ΔT. We can observe the small tertiary clockwise vortices formed around the conducting body inside the main counter-clockwise vortices.

When $\Delta T = 0$ and 0.25 for $Ra = 10^6$, the fluid flow and temperature fields reach the steady state. However, when $\Delta T = 2.5$ and 25 for $Ra = 10^6$, the flow and thermal fields change as a function of time so that isotherms and streamlines shown in Fig. 2(c) and (d) are time-averaged fields. When $\Delta T = 2.5$ for $Ra = 10^6$, both effects of convection caused by the temperature difference between the hot and cold walls and by heat generation from the conducting body have the similar role in the fluid flow and heat transfer in the enclosure. When $\Delta T = 2.5$ for $Ra = 10^6$, the time-averaged streamlines and isotherms show top–bottom and left–right reflectional symmetries unlike to the cases of $Ra \leqslant 10^5$. When $\Delta T = 25$ for $Ra = 10^6$, the effect of convection caused by the heat generation becomes more dominant than that by the hot and cold wall temperature difference. As a result, when $\Delta T = 25$ for $Ra = 10^6$, isotherms ascend upward, a pair of vortices is formed in the enclosure with additional secondary and tertiary vortices, and the time-averaged streamlines and isotherms show a left–right reflectional symmetry, similar to the case of $Ra = 10^5$.

3.1.5. Nusselt numbers at the hot and bottom walls

When $\Delta T = 0.0$ and 0.25, the fluid flow and thermal fields reach the final steady state for different values of $Ra = 10^3$–10^6after they undergo the initial transients. The steady values of surface-averaged Nusselt number at the hot bottom wall, $\overline{Nu}_h$, is the same as those at the cold top wall, $\overline{Nu}_c$, for $Ra = 10^3$–10^6, because isotherms show the diagonally symmetric shape and their surface-averaged thermal gradients at the top and bottom walls are the same as shown in Fig. 2(a). When ΔT increases to 0.25, the effect of free convection caused by the temperature difference between the hot and cold walls on the fluid flow and heat transfer in the enclosure is larger than that caused by heat generation from the conducting body like the case of $\Delta T = 0.0$. As a result, the steady values of surface-averaged Nusselt number at the hot and cold walls for $\Delta T = 0.25$ are almost the same as those for $\Delta T = 0.0$.

When ΔT increases to 2.5, the thermal gradient on the cold wall and $\overline{Nu}_c$ become larger than those at $\Delta T = 0.25$

for $Ra = 10^3$–10^6, because the effect of rising thermal plume caused by the heat generation becomes larger. However, for the case of $\overline{Nu}_h$, the heat generation gives the opposite effect on the bottom hot wall. As a result, when $Ra = 10^3$ for $\Delta T = 2.5$, the value of $\overline{Nu}_h$ at the steady state has a negative value, because the temperature of fluid around the bottom hot wall is larger than the hot wall temperature due to large heat transfer from the conducting body. When the Rayleigh number increases for $\Delta T = 2.5$, the effect of free convection caused by the temperature difference increases with increasing Rayleigh number and the temperature of fluid close to the bottom hot wall becomes smaller than the hot wall temperature. Thus $\overline{Nu}_h$ has positive values at $Ra = 10^4$, 10^5 and 10^6 and increases with increasing Rayleigh number.

When ΔT increases further to 25, the amount of heat generation is very large and the fluid flow and temperature fields are governed by heat generation form the conducting body. Thus $\overline{Nu}_c$ for $\Delta T = 25$ is larger than that for $\Delta T = 2.5$. $\overline{Nu}_h$ for $\Delta T = 25$ has negative values for all Rayleigh numbers considered in the present study and increases with increasing Rayleigh number due to increasing effect of free convection caused by the top and bottom wall temperature difference. When $Ra = 10^6$ for $\Delta T = 25$, the values of $\overline{Nu}_h$ are close to 0, which means that heat from the conducting body is hardly transferred to the hot bottom wall but easily transferred to the cold wall.

When $Ra = 10^6$ for the case of $\Delta T = 2.5$ and $Ra = 10^5$ and 10^6 for $\Delta T = 25$, the fluid flow and temperature fields in the enclosure are time-dependent and as a result $\overline{Nu}_h$ and $\overline{Nu}_c$ have a chaotic pattern as a function of time with large amplitude. The amplitude and frequency of time-dependent surface-averaged Nusselt number are deeply related with the unsteady-motioned shape and location of secondary vortex. It can be well explained by observation of detailed motion of instantaneous velocity and thermal fields. When we compare streamlines and isotherms for the case with large heat generation with those for the case with no or small heat generation at the same Rayleigh numbers, we can recognize that heat generation makes the fluid flow and thermal fields in the enclosure unstable.

Fig. 4 shows the power spectrums of surface-averaged Nusselt number for $\Delta T = 2.5$ and 25 at $Ra = 10^6$. When $\Delta T = 2.5$ for $Ra = 10^6$, the primary frequency of surface-averaged Nusselt number at both hot and cold walls is about 130. However, when ΔT is increased to 25 for $Ra = 10^6$, the power spectrum of $\overline{Nu}_h$ is quite different from that of $\overline{Nu}_c$. The magnitude and primary frequency of power spectrum of $\overline{Nu}_c$ are much larger than those of $\overline{Nu}_c$. The primary frequency of $\overline{Nu}_c$ is about 148. This

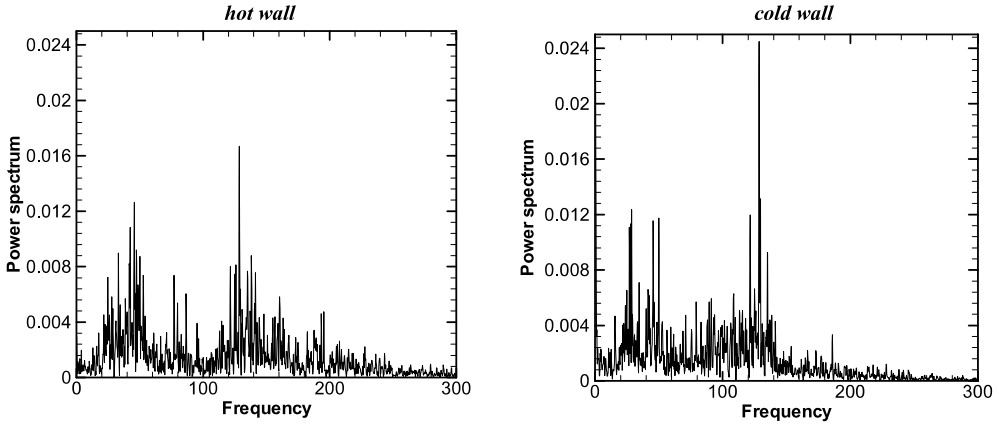

(a) $\Delta T = 2.5$

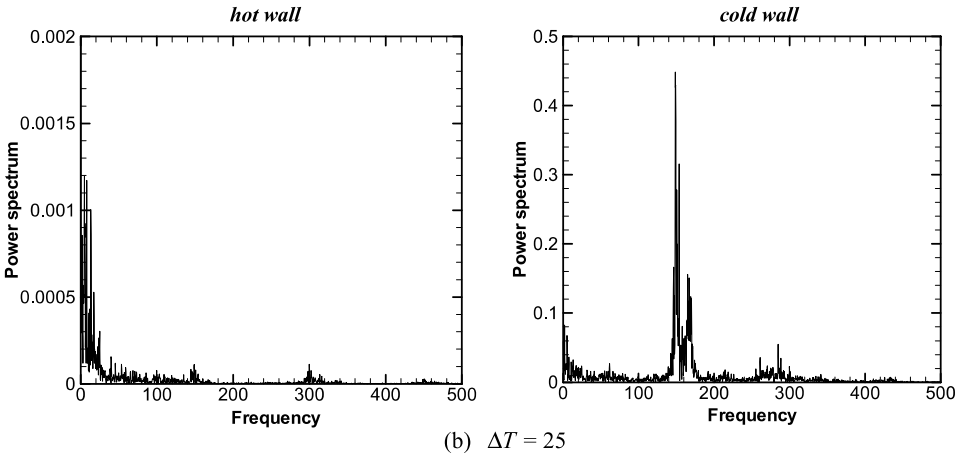

(b) $\Delta T = 25$

Fig. 4. Power spectrum of the surface-averaged Nusselt number at the hot and cold walls for different values of ΔT when $k = 0.1$ and $Ra = 10^6$.

dominant peak value of frequency is corresponding to the phenomenon in which the primary roll cell circulates around the interior body with clockwise and counter-clockwise direction, respectively, so that it changes its direction in reverse repeatedly. Since there is not a primary roll cell circulating around the body but the hot plume which is generated from the body oscillates with its corresponding power spectra. The outstanding frequency on the cold wall has a relation to continuous gross and reduction of secondary vortices at both bottom corners. In fact, since the oscillating plume from the body makes an influence to the downwelling flow moving down through the enclosure next to the body, the periodic change of the shape of secondary vortices is deeply affected by the frequency of hot plume from the body.

3.2. $k = 1$

Fig. 5 shows the time-averaged isotherms and streamlines for different values of ΔT and Rayleigh numbers when $k = 1$. When $k = 1$, the thermal conductivity of fluid is equal to that of conducting body. As the thermal conductivity ratio increases from 0.1 to 1, the thermal resistance of conducting body decreases and heat transfer from the conducting body to the surrounding fluid increases with increasing thermal conductivity ratio. Thus, the values of temperature in the conducting body and in the fluid around the conducting body for $k = 1$ are much smaller than those for $k = 0.1$, as shown in Figs. 2 and 5.

When we compare the results for the distribution of isotherms and streamlines for the case of $k = 1$ with those for $k = 0.1$, the distribution of isotherms and streamlines for $k = 1$ is generally similar to that for $k = 0.1$ for all the Rayleigh numbers considered, except some slight differences around the conducting body due to the difference in the thermal conductivity ratio. However, when $\Delta T = 0.0$ and 0.25 for $Ra = 10^3$, we can observe the striking differences in the distribution of isotherms when we compare isotherms for $k = 1$ with those for $k = 0.1$. When $Ra = 10^3$, heat transfer in the enclosure is dominated by conduction.

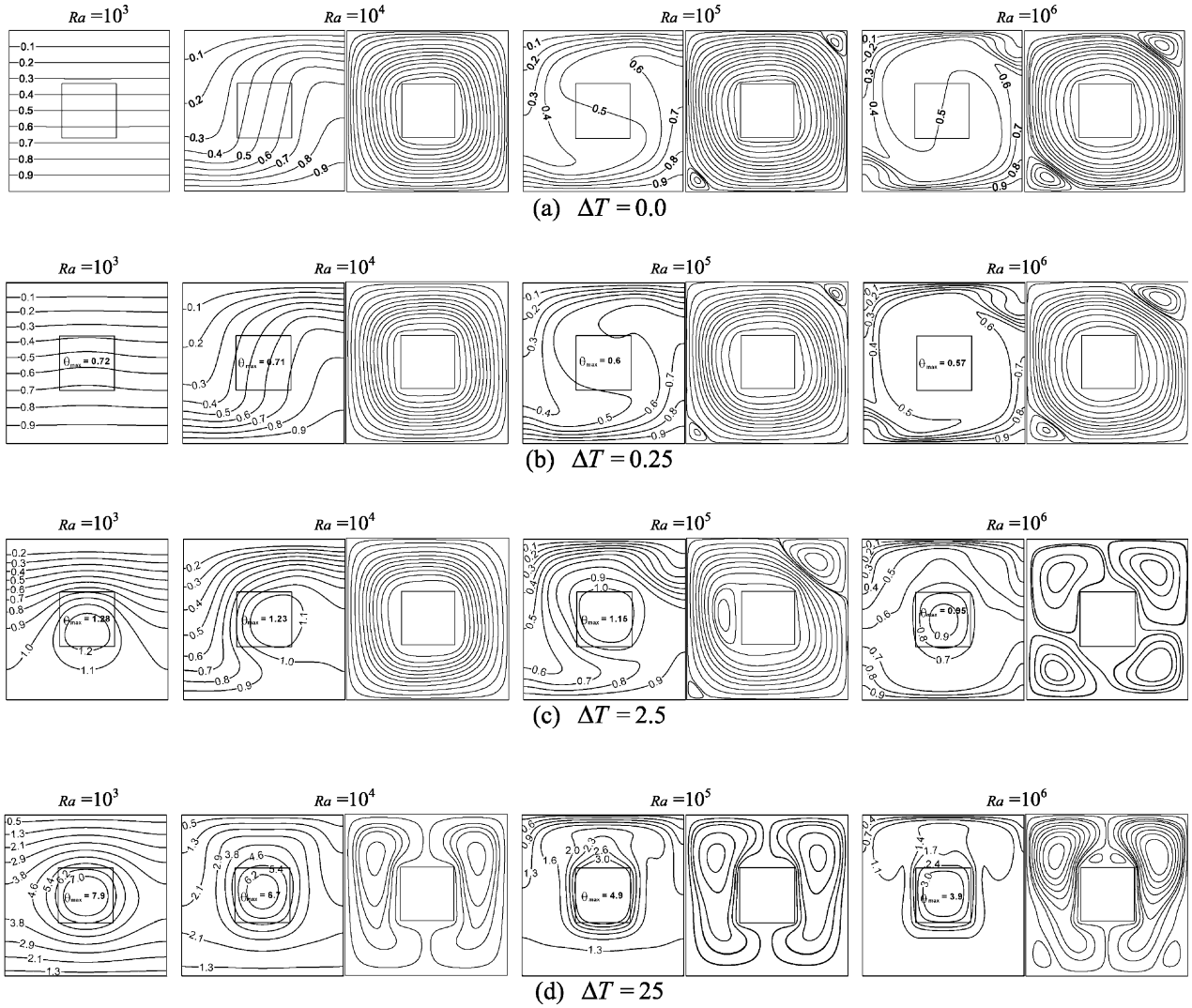

Fig. 5. Time-averaged isotherms and streamlines for different values of ΔT and Rayleigh number when $k = 1$.

Because heat generation from the conducting body is absent or very small when $\Delta T = 0.0$ and 0.25 for $Ra = 10^3$, the conduction heat transfer in the enclosure is mainly governed by the temperature difference between the top and cold walls, the distribution of isotherms is sensitive to the variation of thermal conductivity ratio, and as a result isotherms for $k = 1$ are different from those for $k = 0.1$. When $Ra = 10^3$, the distribution of isotherms for $k = 1$ is almost parallel in the horizontal direction and shows nearly equi-spaced level in the vertical direction, whereas isotherms for $k = 0.1$ move toward the conducting body at the center and shows equi-spaced level at the left and right vertical walls.

Another big difference is observed when $\Delta T = 25$ and $Ra = 10^5$ for different values of $k = 0.1$ and 1. When $k = 1$ with $\Delta T = 25$ and $Ra = 10^5$, the fluid flow and temperature fields are not time-dependent and isotherms and streamlines shown in Fig. 5(d) show the fluid flow and

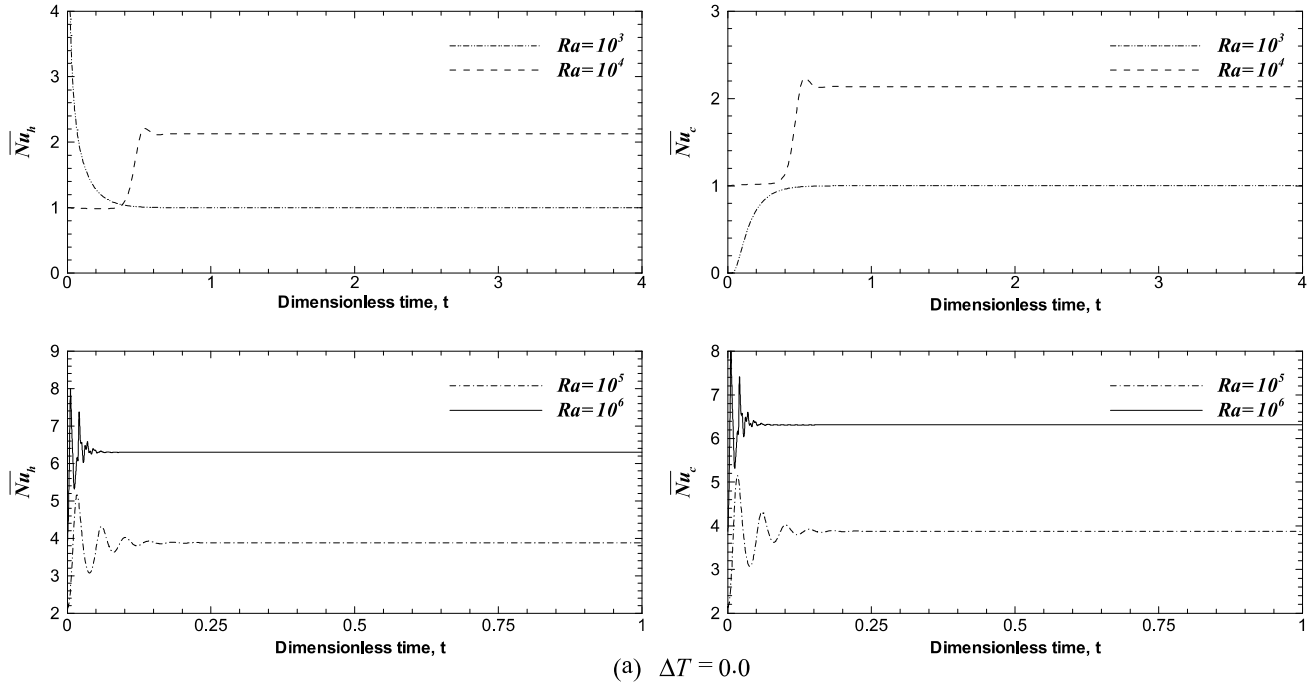

(a) $\Delta T = 0.0$

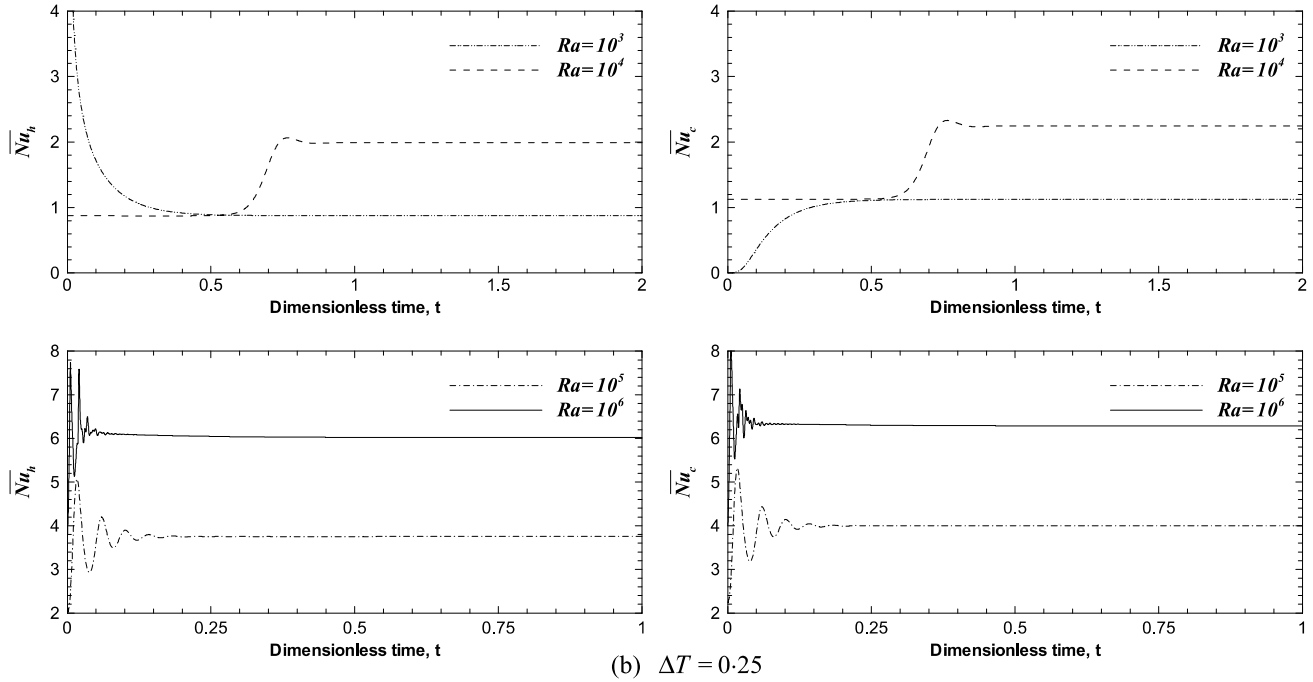

(b) $\Delta T = 0.25$

Fig. 6. Surface-averaged Nusselt number at the bottom hot and top cold walls as a function of time for different values of ΔT and Rayleigh number when $k = 1$.

temperature fields at the steady state. However, when $k = 0.1$ with $\Delta T = 25$ and $Ra = 10^5$, the fluid flow and temperature fields are time-dependent and isotherms and streamlines in Fig. 2(d) show the time-averaged fluid flow and temperature fields. Because thermal gradients at the interface between the fluid and conducting body are the same for $k = 1$, this makes the fluid flow and thermal fields for $k = 1$ more stable than those $k = 0.1$, like the pure Rayleigh–Bénard convection.

Fig. 6 shows the surface-averaged Nusselt number at hot bottom and cold top walls as a function of time for different values of ΔT and Ra when $k = 1$. Similar to the case of $k = 0.1$, the surface-averaged Nusselt number for $k = 1$ increases with increasing Ra. As shown in Figs. 5(a) and (b) and 6(a) and (b), when $\Delta T = 0.0$ and 0.25, the fluid flow and heat transfer characteristics are governed mainly by the free convection caused by the temperature difference between the hot and cold walls and the effect of heat

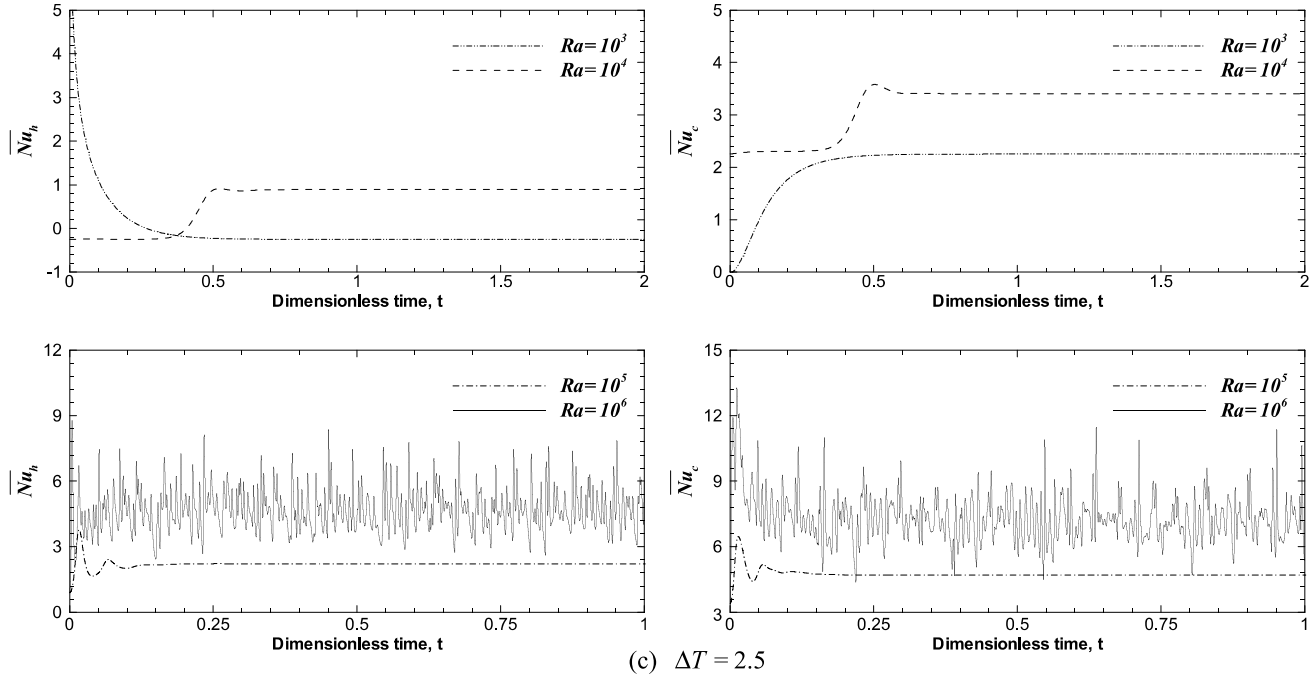

(c) $\Delta T = 2.5$

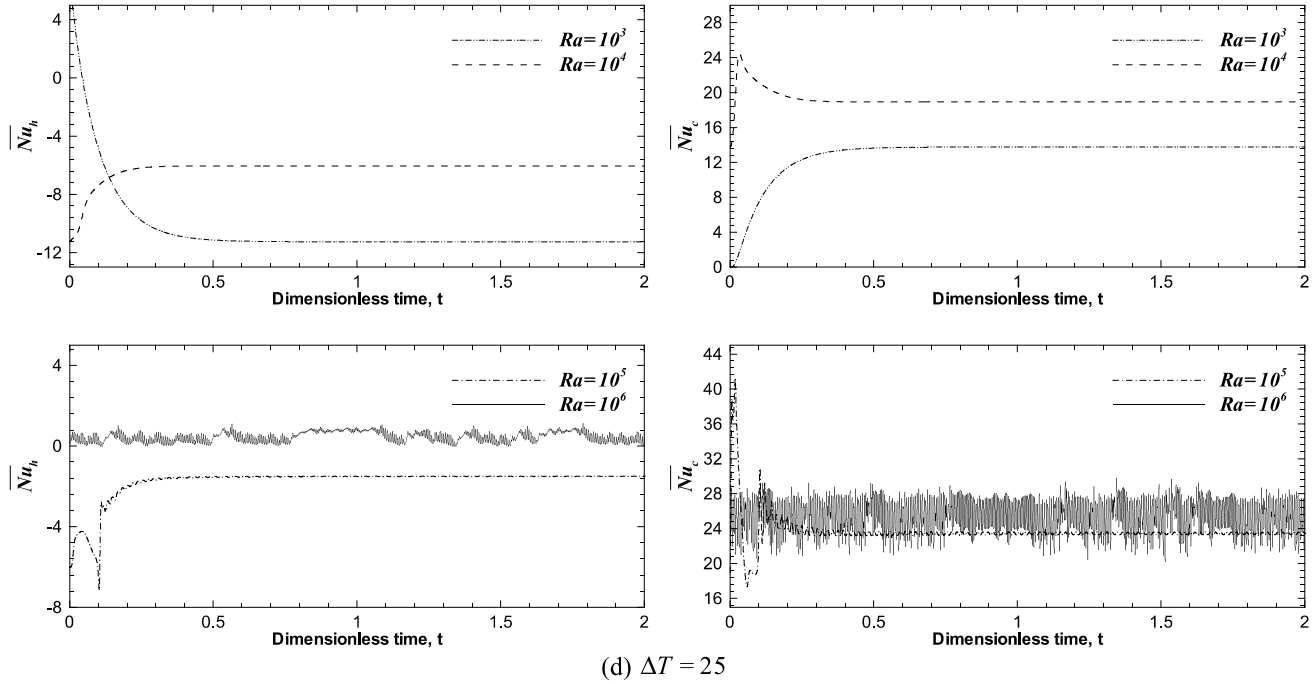

(d) $\Delta T = 25$

Fig. 6 (*continued*)

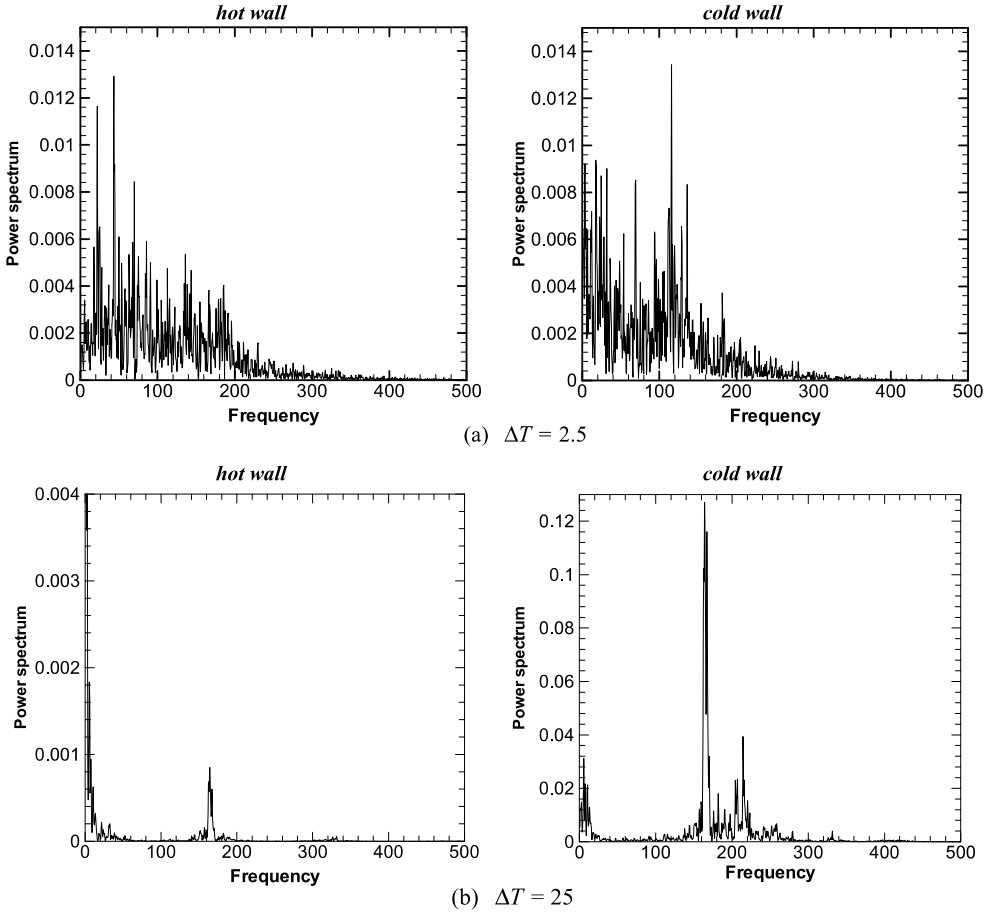

Fig. 7. Power spectrum of the surface-averaged Nusselt number at the hot and cold walls for different values of ΔT when $k = 1$ and $Ra = 10^6$.

generation from the conducting body is not important. The time history of $\overline{Nu_h}$ and $\overline{Nu_c}$ for $\Delta T = 0.25$ is generally similar to that for $\Delta T = 0.0$. When $\Delta T = 0.0$ and 0.25 for $k = 1$, the surface-averaged Nusselt numbers for all Rayleigh numbers of $Ra = 10^3$–10^6 reach the steady state after the initial transient state, as shown in Figs. 6(a) and (b). When ΔT increases to 25, the effect of heat generation becomes very large and $\overline{Nu_h}$ has negative values at some Rayleigh numbers. When $Ra = 10^3$–10^5 for $\Delta T = 2.5$ and $Ra = 10^3$–10^4 for $\Delta T = 25$, the surface-averaged Nusselt number for $k = 1$ also reaches the steady state as explained. However, when $Ra = 10^5$ for $\Delta T = 25$ and $Ra = 10^6$ for both $\Delta T = 2.5$ and 25, the surface-averaged Nusselt numbers for $k = 1$ are time-dependent and oscillates as a function of time, similar to the case of $k = 0.1$. Especially for $Ra = 10^6$ with $\Delta T = 25$, an amplitude of surface-averaged Nusselt number of hot and cold wall looks quite different each other. The amplitude of surface-averaged Nusselt number at the top cold wall is much larger than that at the bottom hot wall. The presence of a conducting body makes the flow in the upper and lower region different. The flow in the upper half enclosure becomes more vigorous due to heat transfer from the heat-generating conducting body, whereas the flow in the lower half enclosure looks stable and as a result the surface-averaged Nusselt number becomes smaller. The power spectrum for the time-dependent surface-averaged Nusselt number at both hot and cold walls for $\Delta T = 2.5$ and $\Delta T = 25$ when $Ra = 10^6$ and $k = 1$ is shown in Fig. 7. The bandwidth of frequency affecting the flow pattern is similar to those for $k = 0.1$. It is noted that these two cases of $\Delta T = 2.5$ and $\Delta T = 25$ at $Ra = 10^6$ show the same flow motion so that the time history of surface-averaged Nusselt number and its power spectrum look similar each other. However, there is a difference in the scale of power spectrum energy. When $k = 0.1$ in which the body acts like adiabatic, the flow is more accelerated and circulates around the conducting body with higher intensity. The faster flow goes, the more frequent and stronger thermal flow is. That is why the spectrum energy for $k = 0.1$ is larger than that for $k = 1$.

3.3. $k = 50$

Fig. 8 shows the time-averaged isotherms and streamlines for different values of ΔT and Rayleigh numbers when $k = 50$. When $k = 50$, the thermal conductivity of fluid is 50 times less than solid thermal conductivity. Since the thermal resistance of conducting body due to conduction is much less than that of surrounding fluid due to convection, the temperature within the conducting body becomes

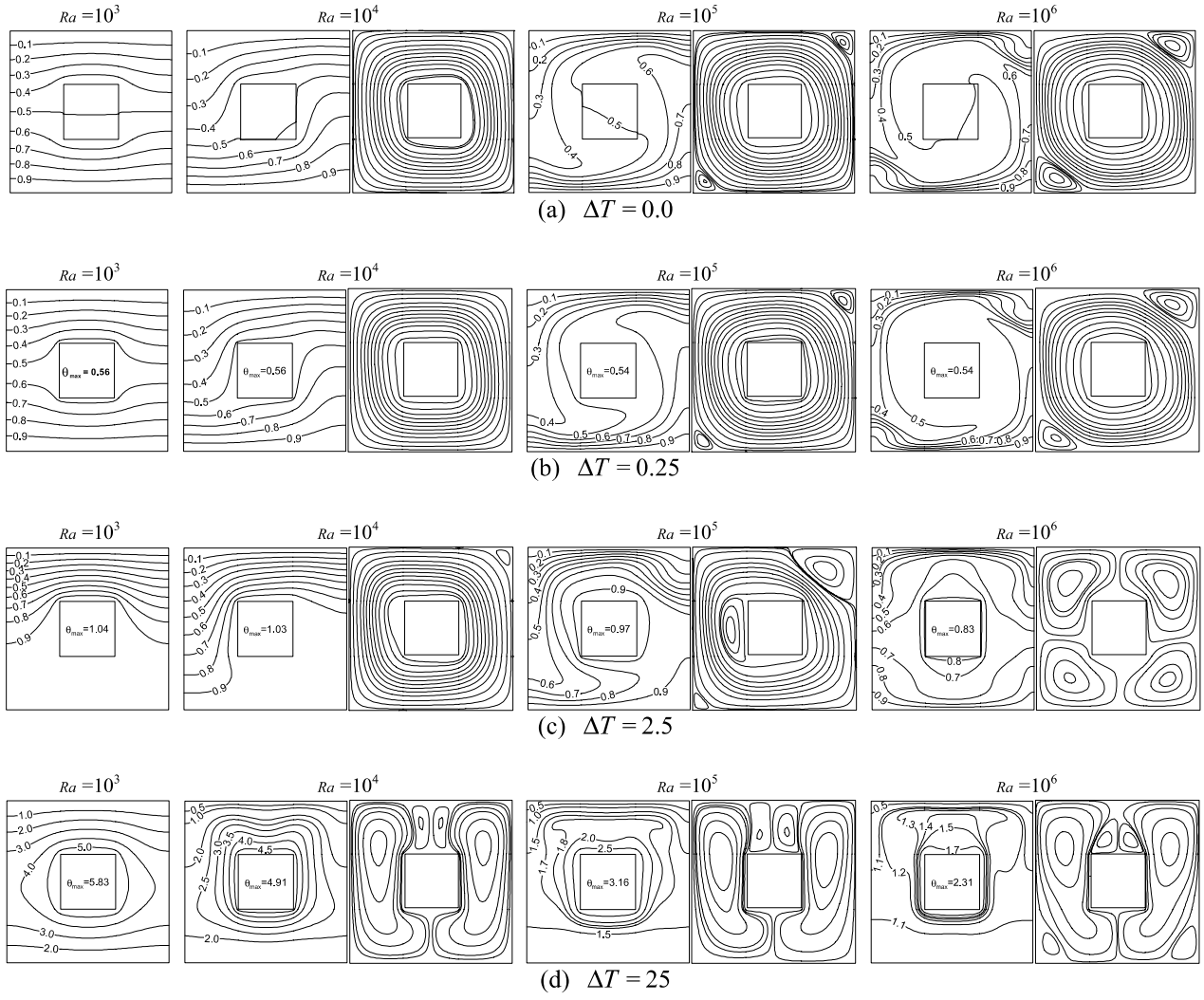

Fig. 8. Time-averaged isotherms and streamlines for different values of ΔT and Rayleigh number when $k = 50$.

almost constant. The maximum temperature for $k = 50$ is lower than that for $k = 0.1$ and 1. However the difference in the maximum temperature between $k = 1$ and $k = 50$ is not large, compared to the large difference in the maximum temperature between $k = 0.1$ and $k = 1$.

When $k = 50$, the general trend in the change of isotherms and streamlines as a function of Ra and ΔT is similar to that for $k = 0.1$ and $k = 1$. However, we can observe some differences for certain Rayleigh numbers and ΔT. When $\Delta T = 0$ and 0.25 for $Ra = 10^3$, the distribution of isotherms depends on the thermal conductivity ratio and the distribution of isotherms for three different values of $k = 0.1$, 1 and 50 shows different distribution. The isotherms at the center for $k = 50$ move away from the conducting body, which is opposite to the distribution of isotherms for $k = 0.1$. Another difference for different values of k is observed when $Ra = 10^4$ and 10^5 with $\Delta T = 25$. When $k = 50$, a pair of secondary vortices that are not observed for $k = 0.1$ and 1 is formed in between a pair of main vortices over the surface of conducting body.

Fig. 9 shows the surface-averaged Nusselt numbers at hot bottom and cold top walls as a function of time for different values of ΔT and Ra when $k = 50$. Fig. 10 shows the power spectrum for the time-dependent surface-averaged Nusselt number at both hot and cold walls for $\Delta T = 2.5$ and $\Delta T = 25$ when $Ra = 10^6$ and $k = 50$. The surface-averaged Nusselt numbers and their power spectrum for $k = 50$ are generally similar to those for $k = 0.1$ and 1. When $\Delta T = 2.5$ and 25 for $Ra = 10^5$, $\overline{Nu}_h$ and $\overline{Nu}_c$ for $k = 0.1$ and 50 are time-dependent, whereas those for $k = 1$ reach the steady state. In Fig. 10(a), we have chosen the only chaotic region of time history of surface-averaged Nusselt number (after 3 in time). Compared with previous two cases ($k = 0.1$ and 1), the bandwidth of dominant frequency of power spectrum is small and less than 100. The flow pattern and its time-averaged field look like those for $k = 0.1$ and 1 but the power spectrum does not. The flow for $k = 50$ is quite more chaotic and the downwelling plume is stronger than the others. That is why the time-history of surface-averaged Nusselt number shows the larger amplitude of higher peak and lower peak and consequently different power spectrum.

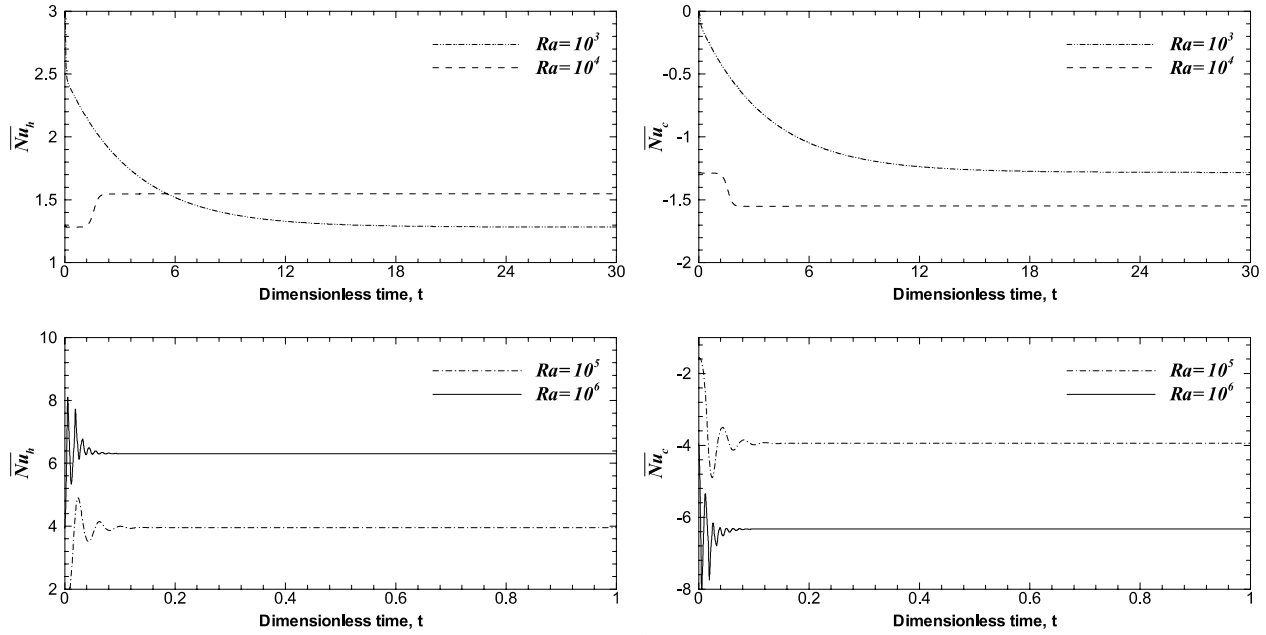

(a) $\Delta T = 0.0$

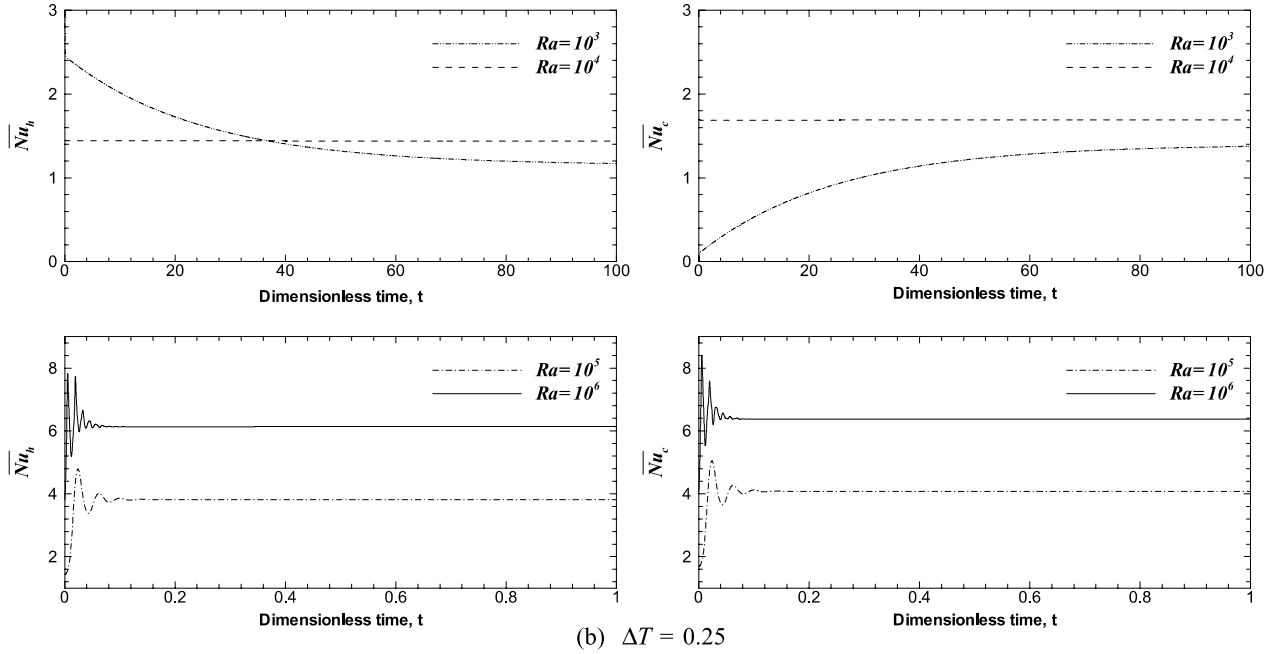

(b) $\Delta T = 0.25$

Fig. 9. Surface-averaged Nusselt number at the bottom hot and top cold walls as a function of time for different values of ΔT and Rayleigh number when $k = 50$.

3.4. Time- and surface-averaged Nusselt number

Fig. 11 shows the time- and surface-averaged Nusselt number at the hot bottom and cold top walls, $\langle \overline{Nu}_h \rangle$ and $\langle \overline{Nu}_c \rangle$, as a function of Rayleigh number for different k and ΔT. When the Rayleigh number increases, the magnitude of velocity increases and as a result $\langle \overline{Nu}_h \rangle$ and $\langle \overline{Nu}_c \rangle$ increase.

When $\Delta T = 0$, 0.25 and 2.5 for $Ra = 10^3$, heat transfer in the enclosure is governed by the conduction mode caused by the temperature difference between the bottom hot and top cold walls. Thus $\langle \overline{Nu}_h \rangle$ and $\langle \overline{Nu}_c \rangle$ for $\Delta T = 0$, 0.25 and 2.5 at $Ra = 10^3$ increase with increasing k from 0.1 to 50 due to the distribution of isotherms shown in Figs. 2, 5 and 8. When ΔT increases to 25 for $Ra = 10^3$, heat transfer is governed by heat generation from the conducting body under the conduction heat transfer mode. As a result $\langle \overline{Nu}_h \rangle$ and $\langle \overline{Nu}_c \rangle$ for different k values of 0.1, 1 and 50 have the almost same value when $\Delta T = 25$ for $Ra = 10^3$.

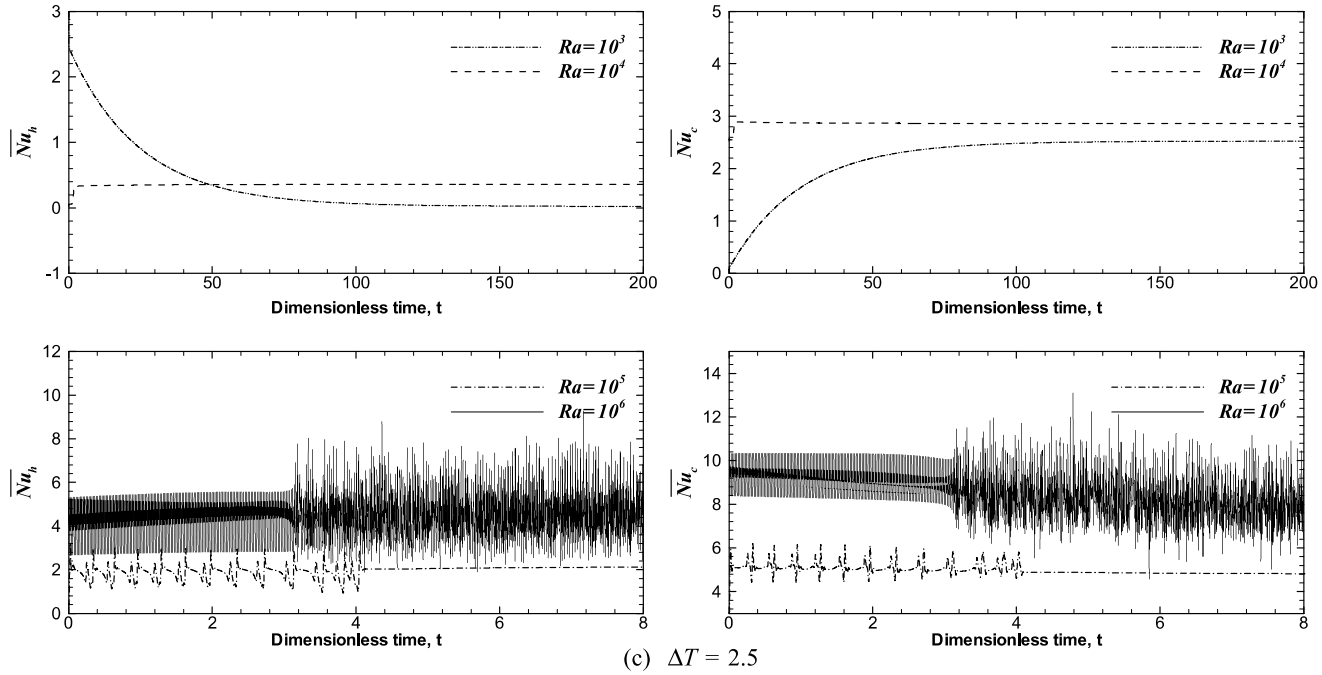

(c) $\Delta T = 2.5$

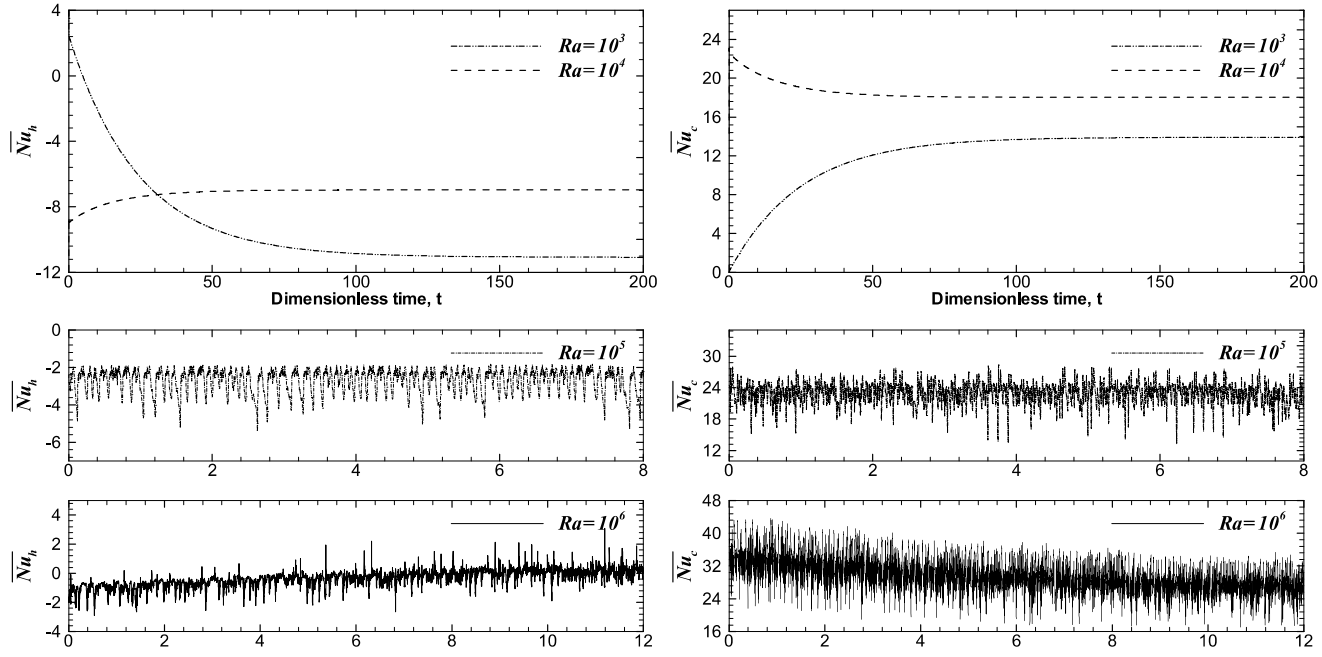

(d) $\Delta T = 25$

Fig. 9 (*continued*)

When $Ra = 10^4$, both heat generation from the conducting body and temperature difference between the bottom and top walls have similar effects on the distribution of fluid flow and temperature fields. Thus, when $\Delta T = 0$, 0.25 and 2.5 for $Ra = 10^4$, $\langle \overline{Nu}_h \rangle$ and $\langle \overline{Nu}_c \rangle$ decrease with increasing k from 0.1 to 50, which is opposite to the case of $Ra = 10^3$. When $\Delta T = 25$ for $Ra = 10^4$, $\langle \overline{Nu}_h \rangle$ and $\langle \overline{Nu}_c \rangle$ also decrease with increasing k, unlike to the case of $Ra = 10^3$ which has almost same values for different k.

When the Rayleigh number increases to 10^5 and 10^6, the effect of temperature difference between two walls becomes larger. Thus, when $\Delta T = 0$, 0.25 and 2.5 for $Ra = 10^5$ and 10^6, isotherms for different k have the similar distribution and their corresponding $\langle \overline{Nu}_h \rangle$ and $\langle \overline{Nu}_c \rangle$ have the almost same values, due to the dominant effects of wall temperature difference on the natural convection in the enclosure. When ΔT increases to 25 for $Ra = 10^5$ and 10^6, we can observe some differences in $\langle \overline{Nu}_h \rangle$ and $\langle \overline{Nu}_c \rangle$ for different values of k, due to dominant effects of heat generation.

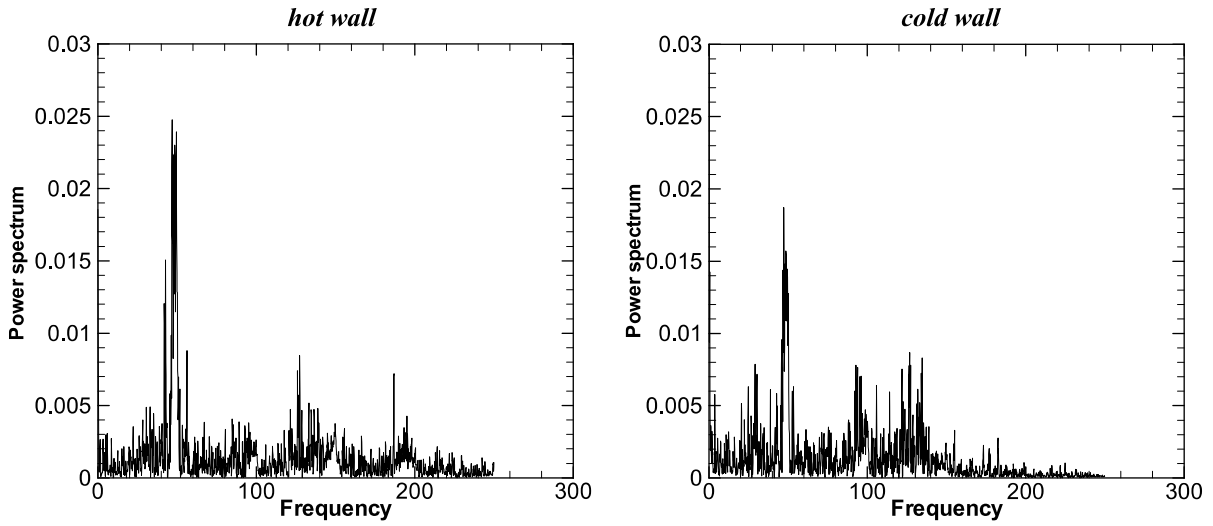

(a) $Ra = 10^6$ and $\Delta T = 2.5$

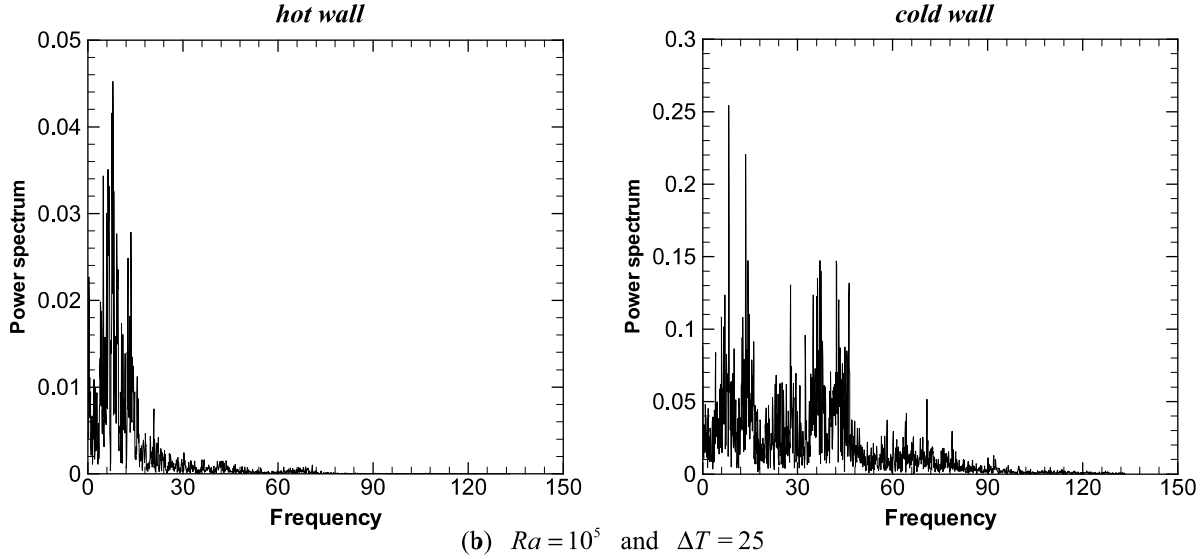

(b) $Ra = 10^5$ and $\Delta T = 25$

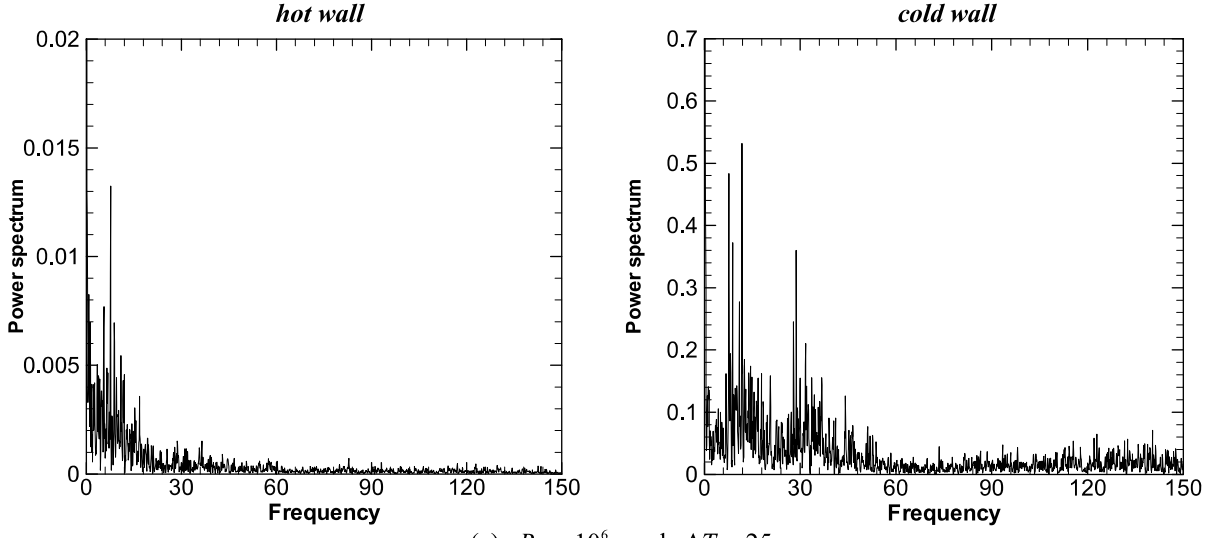

(c) $Ra = 10^6$ and $\Delta T = 25$

Fig. 10. Power spectrum of the surface-averaged Nusselt number at the hot and cold walls for different values of ΔT and Ra when $k = 50$.

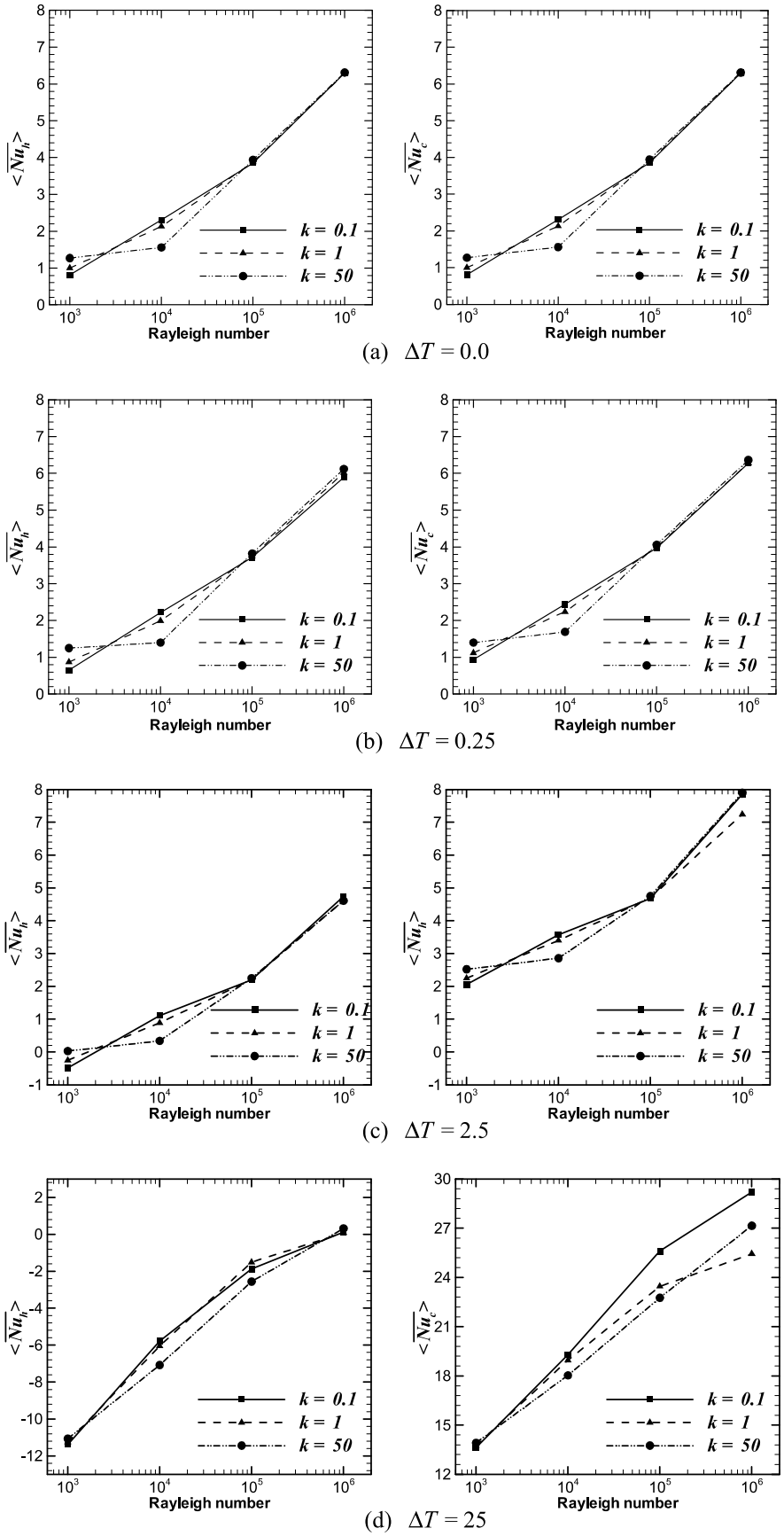

Fig. 11. Time- and surface-averaged Nusselt number at the hot and cold walls as a function of Rayleigh number for different ΔT and k.

When $\Delta T = 25$ for different values of thermal conductivity ratio, $\langle \overline{Nu}_h \rangle$ has negative values for $Ra = 10^3$, 10^4 and 10^5, meaning that the temperature of fluid close to the bottom wall is higher than the bottom hot wall temperature and heat is transferred from the fluid to the bottom hot wall, due to large heat transfer from the heat generating conducting body.

4. Conclusion

We have investigated natural convection in horizontal layer of fluid with heat-generating conducting body in the interior, using an accurate and efficient Chebyshev spectral collocation approach. A multi-domain methodology was employed to address the geometric complexity introduced by the internal body. We make a detailed analysis for the distribution of streamlines, isotherms and Nusselt number as a function of time in order to investigate the effect of unsteadiness and the presence of heat-generating conducting body with different thermal conductivity ratios of $k = 0.1$, 1 and 50 on the fluid flow and heat transfer in the horizontal enclosure for the Rayleigh numbers in the range of $10^3 \leqslant Ra \leqslant 10^6$.

When $\Delta T = 0$ and 0.25, the effect of heat generation from the conducting body is small and the fluid flow and temperature fields in the enclosure are mainly governed by the temperature difference between the bottom hot and top cold walls. When $\Delta T = 0$ and 0.25, streamines and isotherms for all Rayleigh numbers in the range of $10^3 \leqslant Ra \leqslant 10^6$ are not time-dependent and the corresponding Nusselt numbers at the walls reach the steady state after some initial transients. However, because the effects of heat generation on the fluid flow and heat transfer become larger if ΔT increases to 2.5 and 25 and heat generation makes the fluid flow and temperature fields more unstable, streamlines and isotherms for the high Rayleigh numbers of $Ra = 10^5$ and 10^6 become time-dependent and $\overline{Nu}_h$ and $\overline{Nu}_c$ have a chaotic pattern as a function of time with large amplitude.

The distribution of isotherms depends on the thermal conductivity ratio when $\Delta T = 0$, 0.25 and 2.5 because the effect of conduction on heat transfer in the enclosure is larger than convection when $Ra = 10^3$ and 10^4. As a result, with increasing k, $\langle \overline{Nu}_h \rangle$ and $\langle \overline{Nu}_c \rangle$ for $Ra = 10^3$ increase, whereas those at $Ra = 10^4$ decreases. Because the effect of convection on heat transfer in the enclosure is larger than conduction when $Ra = 10^5$ and 10^6, the distribution of isotherms is similar and as a result $\langle \overline{Nu}_h \rangle$ and $\langle \overline{Nu}_c \rangle$ at $\Delta T = 0$, 0.25 and 2.5 have the almost same value for different k values. Because heat transfer is governed by heat generation from the conducting body when $\Delta T = 25$, the distribution of isotherms do not depend on the thermal conductivity ratio and $\langle \overline{Nu}_h \rangle$ and $\langle \overline{Nu}_c \rangle$ have almost same value for $10^3 \leqslant Ra \leqslant 10^6$.

Acknowledgement

This work was partially supported by KOSEF.

References

[1] P.G. Drazin, W.H. Reid, Hydrodynamic Stability, Cambridge University Press, 1981 (Chapter 2).
[2] F.B. Lipps, Numerical simulation of three-dimensional Bénard convection in air, J. Fluid Mech. 75 (1976) 113–148.
[3] S. Balachandar, M.R. Maxey, L. Sirovich, Numerical simulation of high Rayleigh number convection, J. Sci. Comput. 4 (1988) 219–236.
[4] M.Y. Ha, H.S. Yoon, K.S. Yoon, S. Balachandar, I. Kim, J.R. Lee, H.H. Chun, Two-dimensional and unsteady natural convection in a horizontal enclosure with a square body, Numer. Heat Transfer A 41 (2002) 183–210.
[5] J.R. Lee, M.Y. Ha, S. Balachandar, H.S. Yoon, S.S. Lee, Natural convection in a horizontal layer of fluid with a periodic array of square cylinders in the interior, Phys. Fluids 16 (2004) 1097–1117.
[6] J.M. House, C. Beckermann, T.F. Smith, Effect of a centered conducting Body on natural convection heat transfer in an enclosure, Numer. Heat Transfer A 18 (1990) 213.
[7] Q.H. Deng, G.F. Tang, Numerical visualization of mass and heat transport for conjugate natural convection/heat conduction by streamline and heatline, Int. J. Heat Mass Transfer 45 (2002) 2373.
[8] J.Y. Oh, M.Y. Ha, K.C. Kim, Numerical study of heat transfer and flow of natural convection in an enclosure with a heat-generating conducting body, Numer. Heat Transfer A 31 (1997) 289.
[9] M.Y. Ha, M.J. Jung, A numerical study on three-dimensional conjugate heat transfer of natural convection and conduction in a differentially heated cubic enclosure with a heat-generating cubic conducting body, Int. J. Heat Mass Transfer 43 (2000) 4229.
[10] C.L. Streett, M.G. Macaraeg, Spectral multi-domain for large-scale fluid dynamic simulations, Appl. Numer. Math. 6 (1989/1990) 123.
[11] C. Canuto, M.Y. Hussaini, A. Quarteroni, T.A. Zang, Spectral Methods in Fluid Dynamics, Springer Verlag, New York, 1988.
[12] J.R. Lee, M.Y. Ha, A Numerical study of natural convection in horizontal enclosure with a conducting body, Int. J. Heat Mass Transfer 48 (2005) 3308–3318.
[13] S.J. Parker, Stability and vortex shedding of bluff body arrays, PhD thesis, University of Illinois, Urbana, IL, 2002.
[14] G. de Vahl Davis, Natural convection of air in a square cavity: a bench mark numerical solution, Int. J. Numer. Meth. Fluids 3 (1983) 249.